OPEN ACCESS

Metastable Phase Formation in Electrodeposited Co-Rich Co-Cu and Co-Ni Alloys

Journal of The Electrochemical Society, 2023 **170** 062507

Metastable Phase Formation in Electrodeposited Co-Rich Co-Cu and Co-Ni Alloys

M. El-Tahawy,[1,2,3] L. Péter,[1] J. Gubicza,[2] G. Molnár,[4] C. Li,[5] L. Vitos,[1,5,6] and I. Bakonyi[1,z]

[1]*Institute for Solid State Physics and Optics, Wigner Research Centre for Physics. H-1121 Budapest, Hungary*
[2]*Department of Materials Physics, Eötvös Loránd University. H-1117 Budapest, Hungary*
[3]*Physics Department, Faculty of Science, Tanta University. 31527, Tanta, Egypt*
[4]*Institute for Technical Physics and Materials Science, Centre for Energy Research. H-1121 Budapest, Konkoly-Thege út 29-33, Hungary*
[5]*Applied Materials Physics, Department of Materials Science and Engineering, KTH Royal Institute of Technology, Stockholm SE-10044, Sweden*
[6]*Department of Physics and Astronomy, Division of Materials Theory, Uppsala University, Uppsala SE-75120, Sweden*

In a previous work [El-Tahawy et al., *J. Magn. Magn. Mater.* **560**, 169660 (2022)], we reported that from a sulfate type bath, hcp-Co can be electrodeposited at high pH and low current density and investigated the structure and magnetoresistance (MR) characteristics of such hcp-Co electrodeposits. Based on this earlier work, Co-rich Co-Cu and Co-Ni alloy electrodeposits were prepared under the same conditions by adding varying amounts of $CuSO_4$ and $NiSO_4$, respectively, to the $CoSO_4$ bath. According to the results of detailed structural studies by various X-ray diffraction (XRD) geometries, in both the Co-Cu and Co-Ni systems an hcp phase formed exclusively up to about 2 at% of the alloying element. Above this concentration, a significant fcc phase fraction appeared in Co-Cu and a minor fcc fraction in Co-Ni up to about 8 at%. This means that the destabilization effect of Cu on hcp-Co is higher than that of Ni. Although the reduction of the stability of hcp-Co with increasing Cu and Ni content is a well-known phenomenon, a quantitative comparison of this effect in Co-Cu and Co-Ni alloys is missing from the literature. The measured lattice constants are analyzed in comparison with Vegard's law for the Co-Cu and Co-Ni element pairs deduced from data previously reported for the hcp and fcc phases of all three pure elements. For Co-rich Co-Ni alloys, the concentration dependence of the lattice parameters was found to follow Vegard's law for both the hcp and fcc phases due to the miscibility of the two components. For the Co-rich Co-Cu alloys, the data indicate a positive deviation from Vegard's law for both the hcp and fcc phases in agreement with the known similar behavior of fcc Co-Cu alloys for the whole composition range. The positive deviation from Vegard's law in the Co-Cu system is due to the excess mixing volume required for solid solution alloy formation of these immiscible elements in either phases. The MR data are discussed in the light of the observed phases and of the MR parameters reported in our previous work on the hcp and fcc phases of pure Co.

 [DOI: 10.1149/1945-7111/acde64]

Manuscript submitted March 31, 2023; revised manuscript received June 6, 2023. Published June 29, 2023.

The stable phase of pure Co metal exhibits the hexagonal close-packed (hcp) structure at room temperature which transforms to a face-centered cubic (fcc) phase at $T_{hcp \leftrightarrow fcc} = 695$ K.[1] Since the packing density (or atomic volume) of hcp-Co and fcc-Co differs only negligibly[2] and the energy difference between the two phases is also very small,[3] fcc-Co can exist as a metastable phase even at room temperature. For this reason, a Co metal specimen produced by whatever means (e.g., cooling from above $T_{hcp \leftrightarrow fcc}$ to room temperature or prepared via an atom-by-atom deposition process on a substrate) usually may contain some fraction of fcc-Co as well and special efforts are necessary to get pure hcp-Co. Similarly, it is not a trivial task to get pure fcc-Co at room temperature either.

Electrodeposition is a convenient way of getting iron-group metal foils on a conducting substrate.[4] Concerning cobalt, it was revealed already a century ago[5] that electrodeposited Co metal may contain comparable amounts of both the hcp and the fcc phases. In the meantime, it was established from extensive experimental investigations (see, e.g., Ref. 6 and references therein) that the electrodeposition conditions strongly influence the ratio of the two structural modifications in the Co deposit. The general guideline deduced from these investigations[6] was that a high *pH* (about 5) and a low deposition current density (e.g., 5 mA cm^{-2}) favor the formation of the stable hcp-Co phase. The electrolytic deposition at a low rate corresponds to quasi-equilibrium growth in general; no wonder that the equilibrium hcp-Co phase can thus be produced. On the other hand, a bath with low *pH* (between about 2 to 3) and a high deposition current density (e.g., 150 mA cm^{-2}) promote the formation of the fcc-Co phase (of course, some specific details of the deposition conditions may also have an influence on the phases formed).

Along this line, we have recently prepared electrodeposited Co metal foils from a simple $CoSO_4$ bath and studied their magnetic and magnetoresistance (MR) characteristics with special view on revealing a possible difference in the anisotropic magnetoresistance (AMR) of the two Co phases.[7] We have succeeded during that work in the preparation of (i) fully hcp-Co foils at high pH and low current density and (ii) Co foils with predominantly an fcc-Co phase and with a small fraction (about 25%) of an hcp-Co phase at low pH and high deposition current density. A specific outcome of this study was that the AMR ratio could be determined for the first time for the hcp-Co and fcc-Co phases separately. As a new result, it turned out that the AMR ratio is larger by about a factor of 1.8 for the fcc-Co phase than for the hcp-Co phase.

In the present work, we have investigated the phase formation and magnetoresistance characteristics of Co-Cu and Co-Ni alloy electrodeposits prepared under conditions which corresponded to the formation of a hcp phase for pure Co deposits in our previous work.[7] The incorporation of Cu and Ni into Co was achieved by adding varying amounts of $CuSO_4$ and $NiSO_4$, respectively, to the $CoSO_4$ bath. These deposits will be denoted as "hcp"-Co(Cu) and "hcp"-Co(Ni) where the notation "hcp" refers to the deposition conditions of the hcp phase for pure Co deposits. Similar structural studies by various X-ray diffraction (XRD) geometries and MR measurements have been carried out as previously on the pure Co deposits.[7]

The paper is organized as follows. In Experimental section, the preparation details of "hcp"-Co(Cu) and "hcp"-Co(Ni) electrodeposits, the structural characterization methods as well as the magnetoresistance measurement technique will be presented. The experimental results of structural studies by X-ray diffraction (XRD) will

[z]E-mail: bakonyi.imre@wigner.hu

be given in Structural studies of the "hcp"-Co(Cu) and "hcp"-Co(Ni) deposits by XRD section with an analysis of the lattice parameters of the deposits in comparison with Vegard's law. In Magnetoresistance characteristics section, the magnetoresistance data obtained on the electrodeposited foils will be described and analyzed. A summary of the present work will be given in Summary section. In the appendix sections, the literature lattice constant data used for establishing Vegard's law for the Co-Cu and Co-Ni systems are summarized and critically evaluated.

Experimental

Sample preparation.—For the preparation of the "hcp"-Co(Cu) and "hcp"-Co(Ni) electrodeposits, a room-temperature aqueous electrolyte solution containing 100 g l^{-1} $CoSO_4$ (from $CoSO_4{\cdot}7H_2O$, Alfa Aesar) and 45 g l^{-1} H_3BO_3 (Merck) was used. Increasing amounts of $CuSO_4{\cdot}5\ H_2O$ or $NiSO_4{\cdot}5\ H_2O$ were added to this solution in order to introduce more and more Cu or Ni into the deposits. All the solid compounds used were of analytical grade. The *pH* of the solution was regulated to 5.0 by the addition of NaOH.

The "hcp"-Co(Cu) and "hcp"-Co(Ni) layers with a nominal thickness of 5 μm and 3 μm, respectively, were deposited on a Si/Cr(5 nm)/Cu(20 nm) substrate where both the Cr adhesion layer and the Cu substrate layer ensuring a conductive surface were prepared by evaporation on the Si wafer. The nominal thicknesses were obtained by using Faraday's law with 100% current efficiency which was justified by directly measuring deposit thickness with electron microscopy techniques[7] for pure hcp-Co deposits and the same current efficiency should remain valid also for the present "hcp"-Co(Cu) and "hcp"-Co(Ni) deposits as well.

The deposition was performed in a tubular cell with an upward facing cathode completely filling the 8 mm × 20 mm recess at the bottom of the cell in order to ensure the lateral homogeneity of the deposition conditions and to avoid edge effects.[8,9]

Electrodeposition was carried out with direct current at room temperature from the above bath with a current density of 5 mA cm^{-2}.

Chemical analysis on several "hcp"-Co(Cu) deposits was carried out by energy-dispersive X-ray spectroscopy in a TESCAN MIRA3 scanning electron microscope (SEM) equipped with an EDAX Element analyzer. Some small C and O signals were detected for the investigated samples which are very probably surface impurities only (and which are always present in the SEM energy-dispersive X-ray spectra). Besides C and O, neither metallic nor other non-metallic impurities were observed up to the detection limit (about 0.1 at% in our method for elements with atomic number larger than 10) in any of the analyzed samples. The analyzed Cu and Ni contents were obtained by measuring the compositions at four or five locations and the average of these data are specified in Tables I and II up to two decimal digits whereas the standard deviation of these data is about ±0.15 at%.

Investigated samples and their chemical composition.—The "hcp"-Co(Cu) samples investigated in the present study are listed in Table I together with the concentration of copper sulfate of the bath. Since the Cu content was not analyzed for all deposits, the measured Cu content (y) vs bath concentration (x) data were fitted to a second-order polynomial $y = 1.7267\ x^2 + 2.7806\ x$ (the fit quality was fairly good: $R^2 = 0.981$). The column "smoothed Cu content" was derived by using this polynomial for each sample and these data will be used later when discussing the structural and MR data on the present samples. The assessed crystal structure from XRD studies are also specified in Table I. The "hcp"-Co(Ni) samples investigated in the present study are listed similarly in Table II. Since the chemical analysis was carried out for all the "hcp"-Co(Ni) deposits, no smoothing and interpolation was necessary.

It can be seen that the appropriate Ni^{2+} and Cu^{2+} concentrations for achieving the same doping level in the "hcp"-Co(Ni) and "hcp"-Co(Cu) deposits, respectively, differ enormously. This is due to the dissimilar codepositon characteristics of the two doping elements with Co (anomalous codepositon in the Co-Ni system with highly preferred Co deposition and regular codeposition in the Co-Cu system with Cu as the preferentially deposited element[4]).

XRD study.—The phase composition of the Co deposits was investigated by XRD.[10] Since the studied films were not removed from the substrate, the XRD patterns could be measured only in reflection mode. First, the samples were studied in the common Bragg−Brentano (BB) configuration using a Rigaku Smartlab X-ray diffractometer with CuKα radiation (wavelength: $\lambda = 0.15418$ nm) and a 1D D/Tex detector. In this case, divergent beam and symmetrical beam path were applied in the collection of the experimental XRD data. The sample remained horizontal while the X-ray tube and the detector moved at the same rate in the plane of the incident beam and the normal of the sample surface during the experiments. The distance between the sample and the X-ray source was the same as the distance between the detector and the specimen (300 mm). Using BB configuration, only the lattice planes lying parallel to the film surface contribute to the XRD patterns. The measured BB diffractograms revealed that the studied films have crystallographic texture, i.e., one or two reflections are strong while most of the others have very weak intensity or are absent from the patterns which makes the phase identification uncertain. Therefore, additional measurements were performed using parallel-beam (PB) configuration. In this case, the angle between the incident beam and the sample surface was fixed to 10 degrees, therefore the lattice planes not lying parallel to the film surface also contributed to the diffraction patterns. The diffractograms of the specimens were evaluated for the phase composition with the PDXL2 program using the ICDD-2018 database. The XRD studies were carried out on Co (Cu) or Co(Ni) deposits attached to their substrates, therefore in the BB patterns the Si peak can also be seen.

As indicated in Tables I and II, several samples investigated contained both hcp and fcc phases. The relative fraction of the two phases was estimated from the the integrated intensities of the unique peaks for each phase as described in detail in section 3.2.1 of Ref. 7.

The positions of the unique XRD reflections were used for the determination of the lattice parameters. Due to the strong crystallographic texture of the samples, only a few unique peaks were available. Therefore, the lattice constants a_{hcp} and c_{hcp} were determined using the unique hcp peaks $(10\bar{1}0)$and (0002), respectively. For samples from MH-1 to MH-4, the lattice constant c_{hcp} of the hcp phase was determined by the Nelson−Riley extrapolation method using reflections $(10\bar{1}1)$, $(11\bar{2}2)$ and $(20\bar{1}1)$ since reflection (0002) is missing from the XRD pattern due to the texture. As a result, the error of lattice constant c_{hcp} is higher for these samples than for samples MH-5 to MH-11. The lattice constant of the fcc phase was determined from the unique fcc peaks (200) and (222) using the Nelson−Riley method.

Based on the broadening of the XRD peaks, the crystallite size was determined. The physical broadening of the profiles is caused by both the size and strain effects which can be separated by the Williamson-Hall method.[11] Due to the anisotropic (i.e., *hkl* dependent) broadening of the XRD peaks caused by lattice defects such as dislocations and stacking faults, the crystallite size was estimated by analyzing the breadth of a harmonic reflection pair. Thus, for the fcc phase the full width at half maximum (denoted as FWHM with the unit of 1/nm) of peaks (111) and (222) were plotted as a function of the magnitude of the diffraction vector (denoted as g with the unit of 1/nm). Then, a straight line was fitted to the two points on the Williamson-Hall plot and the reciprocal of the intercept of this line with the vertical axis yielded an estimate of the crystallite size. For the hcp phase, the peak pair (100) and (200) was used in the Williamson-Hall plot. Because of the nano-grained microstructure of the studied samples, the physical broadening of the profiles is caused by the size and strain effects and they are much larger than the

Table I. Electrodeposited "hcp"-Co(Cu) samples investigated. For the details of the composition data, see main text. The assessed crystal structure from XRD is also specified (hcp+fcc: a significant fcc fraction is present). Note: the error of chemical analysis data is about ±0.15 at%.

Sample code	$CuSO_4.5H_2O$ concentration in bath (g/l)	measured Cu content (at%)	smoothed Cu content (at%)	smoothed Co content (at%)	structure from XRD
EH-01	0.025		0.07	99.93	hcp
EH-02	0.0375		0.11	99.89	hcp
EH-03	0.05		0.14	99.86	hcp
EH-04	0.06875	0.20	0.20	99.80	hcp
EH-05	0.0875	0.50	0.26	99.74	hcp
EH-06	0.11875		0.35	99.65	hcp
EH-07	0.15625		0.48	99.52	hcp
EH-08	0.21875	0.65	0.69	99.31	hcp
EH-09	0.3125	1.13	1.04	98.96	hcp
EH-10	0.64	3.33	2.49	97.51	hcp+fcc
EH-11	1.238	6.57	6.09	93.91	hcp+fcc
EH-12	1.83	9.15	10.87	89.13	hcp+fcc
EH-13	2.368	17.10	16.27	83.73	hcp+fcc

Table II. Electrodeposited "hcp"-Co(Ni) samples investigated. The assessed crystal structure from XRD is also specified (hcp(+fcc): these samples probably contain an fcc phase fraction; hcp+fcc: a significant fcc fraction is present). Note: the error of chemical analysis data is about ±0.15 at%.

Sample code	$NiSO_4.5H_2O$ concentration in bath (g/l)	Measured Ni content (at%)	Measured Co content (at%)	Structure from XRD
MH-1	10.2	0.95	99.05	hcp
MH-2	20.4	1.20	98.80	hcp
MH-3	30.6	1.88	98.12	hcp
MH-4	47.6	2.27	97.73	hcp(+fcc)
MH-5	68.0	2.98	97.03	hcp(+fcc)
MH-6	88.4	3.60	96.40	hcp(+fcc)
MH-7	136	5.36	94.64	hcp(+fcc)
MH-8	170	6.36	93.64	hcp(+fcc)
MH-9	204	8.16	91.84	hcp(+fcc)
MH-11	238	8.50	91.50	hcp+fcc

instrumental broadening. Therefore, instrumental correction was not applied in the evaluation.

Measurement of the magnetoresistance characteristics.—For the magnetoresistance measurements, the whole deposit (8 mm × 20 mm) on its Si/Cr/Cu substrate was used. Since the deposits were 3 μm or 5 μm thick, the shunting effect of the thin Cr and Cu underlayers could be neglected. The resistivity of the Co deposits was measured by applying a d.c. current along the longer edge of the deposit in a four-point-in-line probe with flat gold-coated spring contacts which were sufficiently wide to ensure a homogeneous current distribution over the whole width of the deposits.

The MR measurements were performed at room temperature in the current-in-plane and field-in-plane configuration in magnetic fields up to $H = 8$ kOe. The MR ratio at a magnetic field H was defined with the formula $MR(H) = \Delta R/R_o = [R(H) - R_o]/R_o$ where $R(H)$ is the resistance in an external magnetic field H and R_0 is the resistance maximum/minimum close to zero magnetic field. The MR (H) curves were measured with two orientations of the magnetic field with respect to the current: field parallel to the current flow (longitudinal MR = LMR) and field perpendicular to the current flow (transverse MR = TMR). The saturation values of the longitudinal and transverse MR components (LMR_s and TMR_s, respectively) were obtained by an extrapolation of the MR(H) data from the magnetically saturated (single-domain) region to $H = 0$.[7] The anisotropic magnetoresistance (AMR) ratio is defined as AMR = LMR_s—TMR_s.

Structural Studies of the "hcp"-Co(Cu) and "hcp"-Co(Ni) Deposits by XRD

Evolution of the phase constitution of the "hcp"-Co(Cu) deposits with the Cu content.—According to the XRD studies, samples EH-01 to EH-09 (i.e., those with a Cu content below 2 at%; see Table I) did not contain any fcc phase fraction but were composed of an hcp phase only. This is demonstrated by the XRD patterns for sample EH-08 (0.69 at% Cu) in Fig. 1 which were recorded in the BB geometry (left panel) and in the PB geometry (right panel). Only unique hcp peaks (vertical solid-line arrows) close to the corresponding pure hcp-Co line positions[12] can be observed, whereas there are no unique fcc peaks (expected positions for pure fcc-Co[13] are indicated by the vertical dashed-line arrows). Furthermore, several coinciding hcp/fcc peaks are also indicated. The BB pattern also reveals the substrate Si(400) peak. The vertical red solid lines on the BB pattern indicate the positions of the bulk fcc-Cu(111) and fcc-Cu(200) reflections[14] and the lack of peaks at these positions is a strong evidence for the absence of a pure fcc-Cu phase.

The observed XRD patterns demonstrate that below 2 at% Cu, the "hcp"-Co(Cu) deposits constitute a single-phase solid solution of Cu in hcp-Co.

When further increasing the Cu content to 2.49 at% (sample EH-10) and beyond in the "hcp"-Co(Cu) deposits, the XRD patterns exhibited, besides the hcp phase reflections, also an evidence of a minor fcc phase fraction. First, the relative intensities of the coincident reflections hcp(0002)/fcc(111), hcp $(11\bar{2}0)$/fcc(220) and hcp $(11\bar{2}2)$/fcc(311) increased (this intensity change could be more pronouncedly observed in the PB patterns). Second, unique fcc-Co (200) and fcc-Co(222) peaks clearly appeared both in the BB and PB patterns. Furthermore, the relative intensities of the unique hcp reflections were strongly reduced.

The evolution of the relative intensities of the two phases with increasing Cu content can be clearly observed in Fig. 2 when comparing the PB patterns for sample EH-10 (2.49 at% Cu) and EH-13 (16.27 at% Cu). For the largest Cu content (EH-13), the unique hcp reflections are strongly reduced, some of them are almost invisible. Hence, the pattern is dominated, in addition to a clear unique fcc-(200) peak, by the coincident hcp/fcc peaks which are certainly attributable to an fcc phase. Still, no pure fcc-Cu phase seems to be present.

The absence of the fcc-Cu(111) and fcc-Cu(200) peaks in the XRD patterns up to the highest Cu content investigated (16.27 at%) means that the "hcp"-Co(Cu) deposits do not contain a detectable separate fcc-Cu phase. Since the fcc phase appears only above 2 at% Cu, up to this Cu content the codeposited Cu atoms are probably in a solid solution state in hcp-Co. As will be shown later, for Cu contents around 2 at%, the crystallite size reduces down to about 20–30 nm for both phases and for higher Cu contents even down to 10 nm. The nanocrystalline regime is known to significantly increase the solid solubility and this can explain the absence of a separate Cu phase up to the highest Cu contents.

Evolution of the phase constitution of the "hcp"-Co(Ni) deposits with Ni content.—According to the XRD studies, all the "hcp"-Co(Ni) samples listed in Table I consisted predominantly of an hcp Co-Ni phase.

For Ni contents up to about 2 at%, neither the BB nor the PB pattern indicated the presence of unique fcc peaks as demonstrated for sample MH-3 (1.88 at% Ni) in the left panel of Fig. 3 where we can observe four unique hcp peaks and two coincident hcp/fcc peaks. On the other hand, the XRD pattern recorded in the same geometry for sample MH-4 (2.27 at% Ni) on the right panel of Fig. 3 reveals a very small fcc(200) peak and a peak also appears at the position of the hcp(0002)/fcc(111) coincident reflection pair. Otherwise, the two patterns display the same Bragg peaks.

The lack of fcc(200) and fcc(222) peaks below about 2 at% Ni indicate that these "hcp"-Co(Ni) samples do not contain an fcc phase. After exceeding this Ni content, a very small fraction of an fcc phase appears as indicated by the small fcc(200) reflection peak, and the emerging small hcp(0002)/fcc(111) coincident reflection pair may also hint at the presence of a tiny fcc fraction. These peaks with

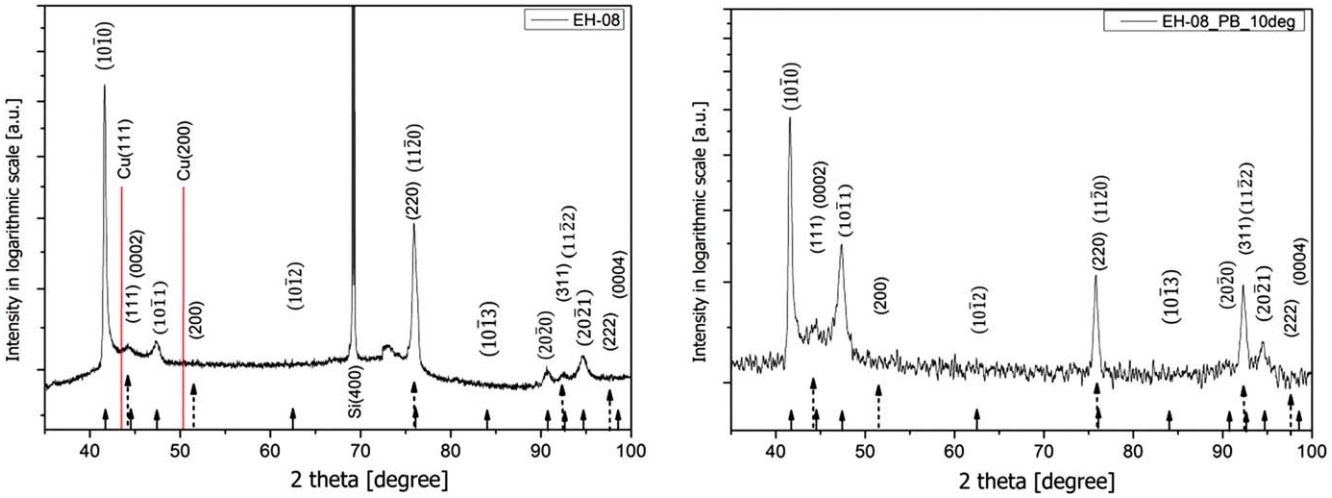

Figure 1. XRD patterns of sample EH-08 (0.69 at% Cu) measured in the BB (left panel) and PB (right panel) geometries. The vertical solid and dashed arrows indicate the positions of the specified Bragg reflections of the hcp-Co and fcc-Co phases, respectively. The vertical red lines in the BB pattern indicate the expected positions of the fcc-Cu(111) and fcc-Cu(200) reflections.

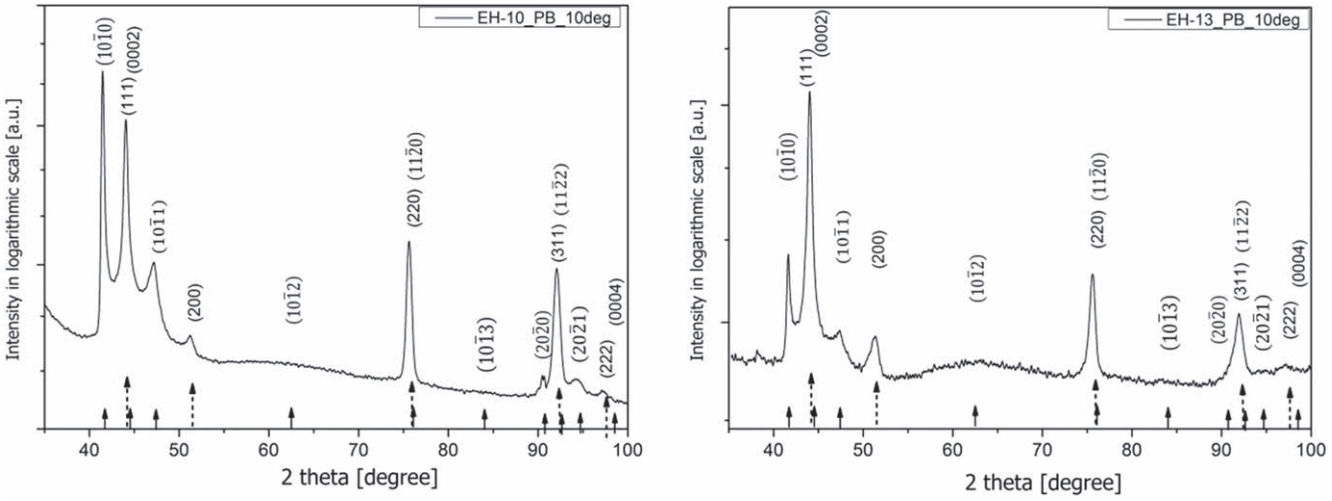

Figure 2. XRD patterns measured in the PB geometry for sample EH-10 (6.09 at% Cu) on the left panel and for sample EH-13 (16.27 at% Cu) on the right panel. The vertical solid and dashed arrows indicate the positions of the specified Bragg reflections of the hcp-Co and fcc-Co phases, respectively.

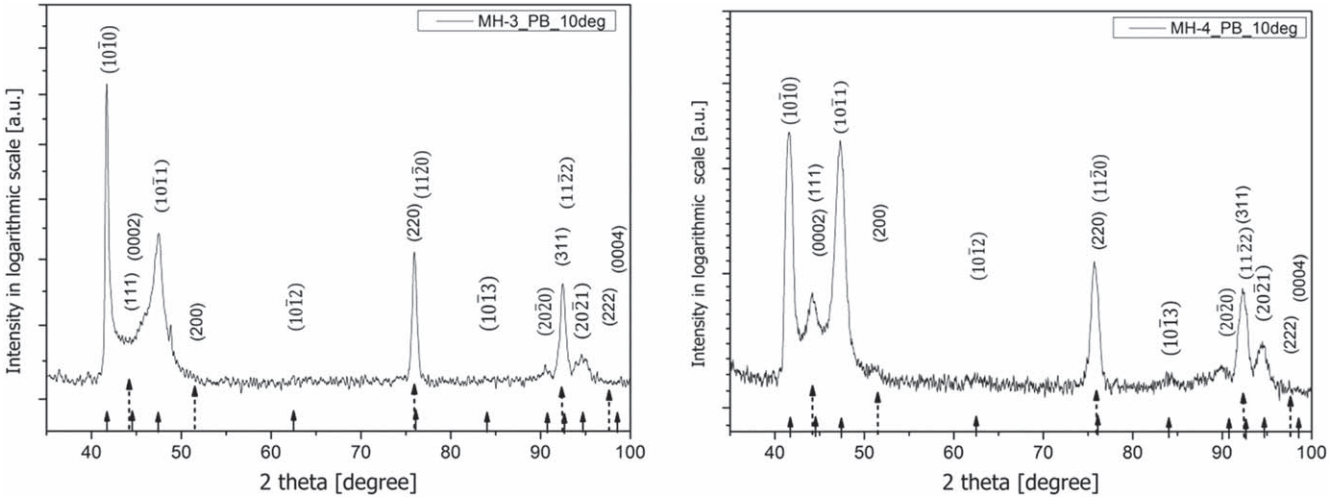

Figure 3. XRD patterns measured in PB geometry for sample MH-3 (1.88 at% Ni) (left panel) and sample MH-4 (2.27 at% Ni) (right panel). The vertical solid and dashed arrows indicate the positions of the specified Bragg reflections of the hcp-Co and fcc-Co phases, respectively.

low intensity appear for several samples both in the BB and PB patterns.

With further increase of the Ni content, the XRD patterns remain essentially the same and are dominated by the hcp peaks. The relative intensity of the fcc(200) peak remains fairly small; however, the relative intensity of hcp(0002)/fcc(111) coincident peak slightly increases with Ni content. This is shown for sample MH-8 (6.36 at% Ni) for which the PB pattern (left panel of Fig. 4) reveals a small fcc (200) peak besides a significantly enhanced hcp(0002)/fcc(111) coincident peak. The right panel in Fig. 4 shows the XRD pattern for sample MH-11 with the highest Ni content (8.5 at%) where the hcp(0002)/fcc(111) coincident peak has already an intensity higher than the main hcp peak ($10\bar{1}0$). In addition, we can also observe here the unique fcc(200) and fcc(222) peaks and a high intensity of the hcp ($11\bar{2}2$)/fcc(311) coincident peak. All these features mean that, besides the hcp phase, there is a comparable amount of an fcc phase in the deposit with the highest Ni content.

The absence of an fcc-Ni(111) peak corresponding to the standard lattice constant $a_{\text{fcc-Ni}}$[15] in the XRD patterns up to the highest Ni content investigated (8.5 at%) means that the "hcp"-Co (Ni) samples do not contain a detectable separate fcc-Ni phase. Therefore, the codeposited Ni atoms should form a solid solution with both hcp-Co and fcc-Co at least up to the highest Ni contents investigated. Unfortunately, we have no information on the actual Ni contents in either of the hcp or fcc phases.

Phase fractions, crystallite size and microstrain of the investigated deposits.—According to Tables I and II in which the phase identification was based on the evaluation of the XRD patterns as discussed in Evolution of the phase constitution of the "hcp"-Co(Cu) deposits with the Cu content and Evolution of the phase constitution of the "hcp"-Co(Ni) deposits with Ni content sections, the appearance of the constituting phases can be summarized as follows.

In both the "hcp"-Co(Cu) and "hcp"-Co(Ni) deposits, a single hcp phase was only observed up to about 2 at% of the alloying element. Above about 2 at%, in both alloy systems an fcc phase also appears. The fcc fraction is considerable in the Co-Cu system, continuously increasing with Cu content as shown by the full triangle symbols in Fig. 5 and it reaches about 50% for the highest Cu content investigated. On the other hand, in the Co-Ni system the fcc fraction is fairly small up to about 8 at% Ni so that it can hardly be quantified. However, by about 8.5 at% Ni, the fcc fraction (see full square symbols in Fig. 5) suddenly rises to 38% and it becomes equal to the fcc fraction in the Co-Cu deposits at the same alloying element concentration.

It can be established from these data that in the deposits prepared under the present conditions, the hcp phase of Co can dissolve about 2 at% Cu and at least about 8 at% Ni in its lattice without the formation of a considerable fraction of the fcc phase. This is in agreement with the equilibrium phase diagrams of the two systems[1] according to which, in comparison with Cu, the room-temperature solubility of Ni is much higher for the hcp-Co phase, the solubility limit being as high as about 30% Ni. The larger solubility limit for Ni is due to the stronger similarity of the electronic structure and atomic size with Co than that of Cu with Co.

As to the crystallite size deduced from the Williamson-Hall plots, we recall that for pure hcp-Co deposits a crystallite size of about 900 nm was estimated in our previous work[7] (it should be noted that this is the upper limit for deducing crystallite size from XRD). Figure 5 indicates that adding even a few atomic percents of either Cu (open diamonds) or Ni (open circles) to the Co deposits, the crystallite size reduces drastically, at least by a factor of 2 and then by more than an order of magnitude for the highest alloying element concentrations. The overall crystallite size evolution with composition is practically the same for both Cu and Ni and it does not differ either for the constituent hcp and fcc phases. The very small crystallite sizes appear especially in the mixed-phase region. Interestingly, we have made the same observation also for pure Co electrodeposits containing both hcp and fcc phases.[7]

Figure 6 summarizes the microstrain data from the Williamson-Hall analysis for both the hcp and fcc phases of the investigated deposits. There seems to be no significant difference in the data either for the Co-Cu and Co-Ni deposits or for the hcp and fcc phases. Starting from the values obtained for the hcp-Co and fcc-Co phases in our previous work,[7] the present data indicate a continuous increase by about a factor of 2 with increasing alloying element concentration.

The enhancement of microstrain with increasing alloying element concentration is most probably related to the refinement of the microstructure (see Fig. 5). A fraction of boundaries separating the crystallites is most probably semi-coherent or incoherent which contain lattice defects, such as dislocations. The strain field of these defects contributes significantly to the microstrain measured from the analysis of the diffraction peak breadth. Thus, a smaller crystallite size is associated with a higher amount of boundaries, resulting in a larger microstrain with increasing alloying element concentration.

Lattice constants and average atomic volume of the hcp and fcc phases in the deposits.—After having a picture about the phase constitution of the "hcp"-Co(Cu) and "hcp"-Co(Ni) alloy deposits,

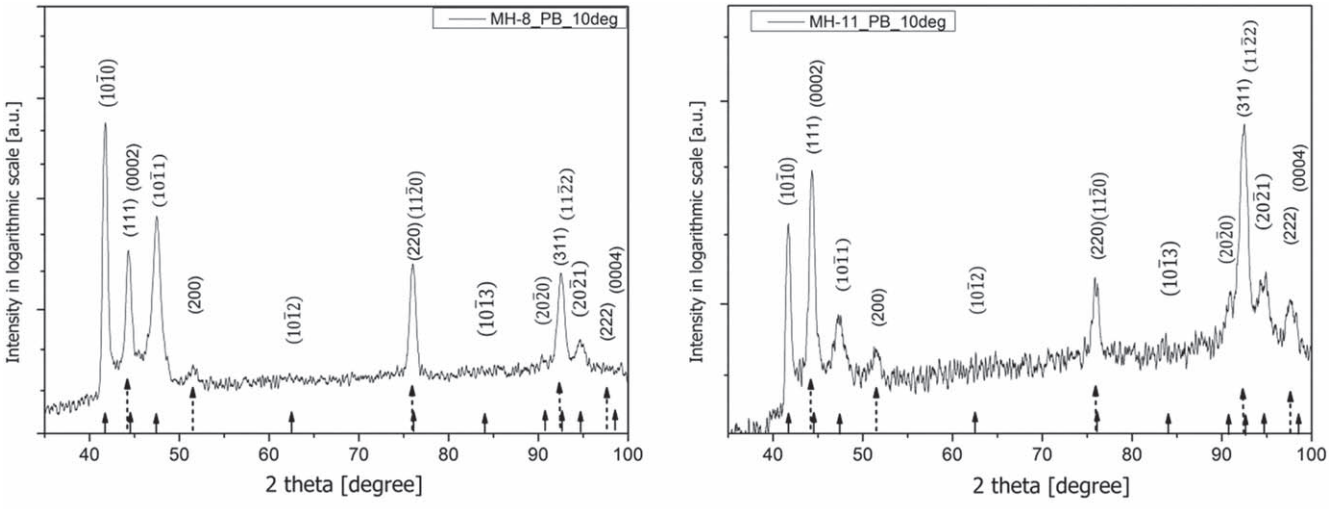

Figure 4. XRD patterns of sample MH-8 (6.36 at% Ni) (left panel) and sample MH-11(8.5 at% Ni) (right panel), both measured in the PB geometry. The vertical solid and dashed arrows indicate the positions of the specified Bragg reflections of the hcp-Co and fcc-Co phases, respectively.

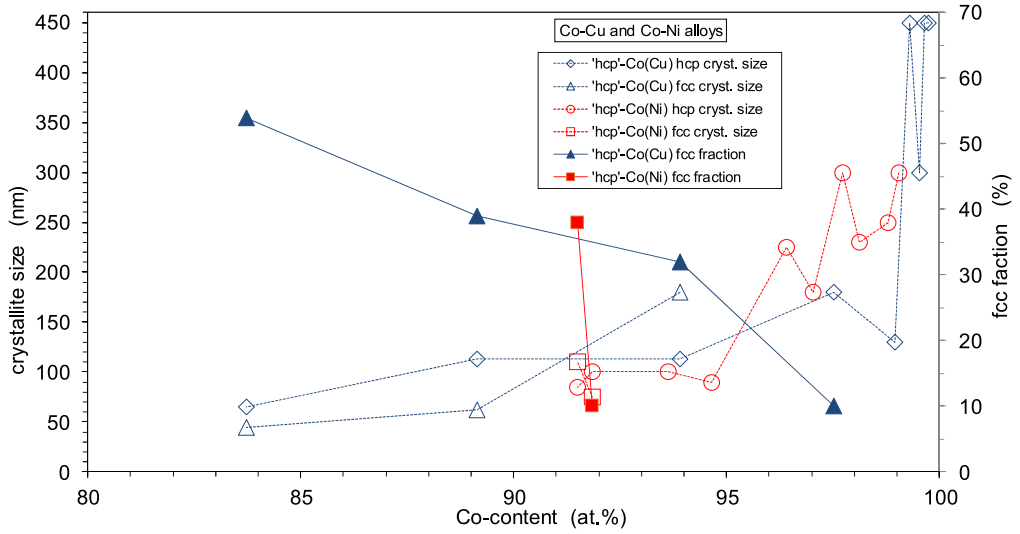

Figure 5. Composition dependence of the crystallite size of the constituent hcp and fcc phases (open symbols, left axis) and the fcc phase fraction (solid symbols, right axis) in the Co-Cu and Co-Ni deposits.

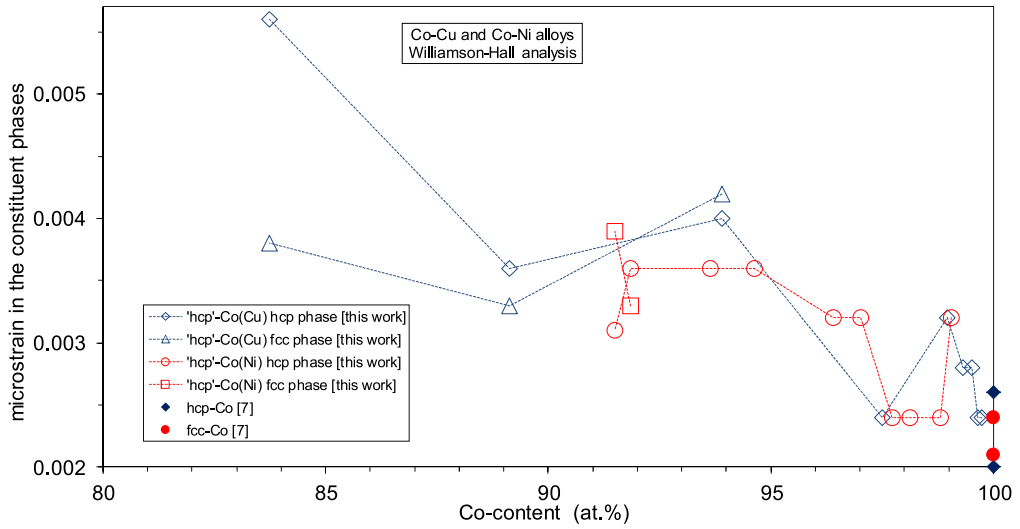

Figure 6. Variation of the microstrain with composition in the hcp and fcc phases in the Co-Cu and Co-Ni deposits as deduced from the Williamson-Hall analysis.

we shall now turn attention to an evaluation of the lattice parameters of the two phases in these samples and their variation with Cu and Ni content. The composition variation of the lattice parameters will be performed in view of Vegard's law based on the lattice parameters of the corresponding phases of the constituent elements. These lattice parameters and the Vegard's law for both phases of the two alloy systems are summarized in the Appendices.

The variation of the lattice constants and the average atomic volume with Cu content of the "hcp"-Co(Cu) alloy deposits is shown in Fig. 7. As discussed in appendix C, the lattice constants a_{hcp} and c_{hcp} of pure hcp-Co electrodeposits is typically below and above, respectively, the corresponding standard values of hcp-Co. This was assigned there to the fact that due to the strong texture and small grain size of the electrodeposits, the rather few and low-intensity XRD peaks do not allow the same systematic correction of the measured line positions as it could be done for bulk hcp-Co.[16] Apparently, the situation is the same also for all the investigated "hcp"-Co(Cu) alloy deposits. As to the lattice constant a_{hcp} (Fig. 7a), if we shift upwards the alloy data to a level where the samples with low Cu content reach the standard value, we can see that with increasing Cu content, an overall slight increase beyond the Vegard line can be observed. Such an excess increase can be observed also for the data on c_{hcp} (Fig. 7b) and V_{hcp} (Fig. 7c): the dashed straight lines over these data which show their overall trends definitely have a higher slope than the corresponding Vegard line.

This behavior corresponds to the discussion in connection with Fig. A.6 in the appendix according to which solid solution in the Co-Cu system can only form with an excess volume both in the hcp and the fcc phases.

It should be kept in mind that this excess volume is fairly small in Fig. 7c due to the limited Cu content (about 2.5 at%) that could be incorporated in the present "hcp"-Co(Cu) deposits with the possibility of structurally evaluating the hcp phase.

The variation of the lattice constants and the average atomic volume with Ni content of the "hcp"-Co(Ni) alloy deposits is shown in Fig. 8. Similarly to the "hcp"-Co(Cu) alloy deposits, the lattice parameter a_{hcp} for the "hcp"-Co(Ni) alloy deposits is slightly below and the lattice parameter c_{hcp} and the average atomic volume V_{hcp} are slightly above the corresponding Vegard lines. This is again due to the difference in the evaluation procedure of the lattice parameter data with respect to the evaluation of the bulk XRD data.

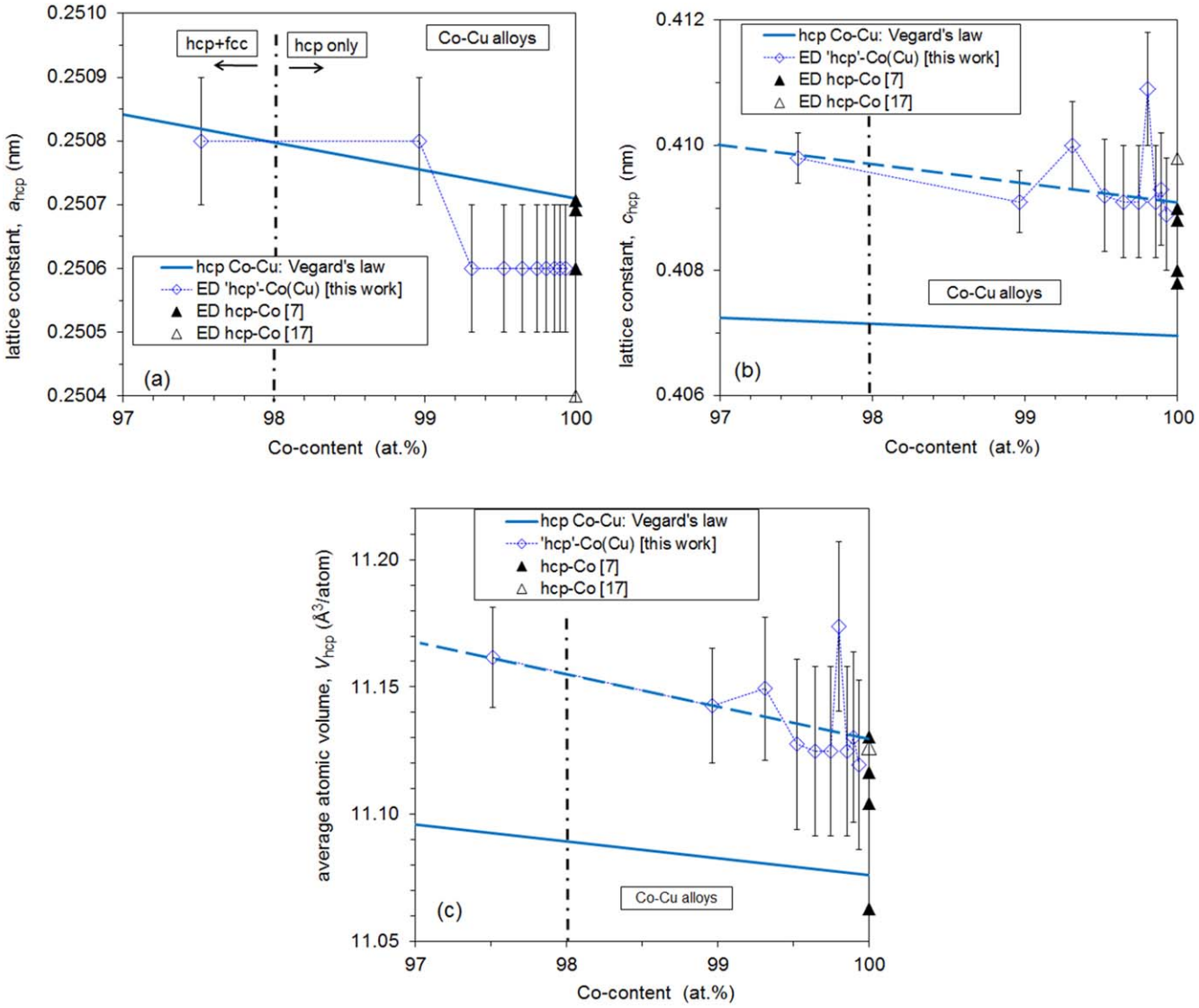

Figure 7. Lattice constants a_{hcp} (a) and c_{hcp} (b) and average atomic volume V_{hcp} (c) of the hcp phase in the "hcp"-Co(Cu) (◇) electrodeposits. Previous results for pure electrodeposited hcp-Co are also added (▲[7] and Δ[17]). The solid line corresponds to Vegard's law for the hcp phase in the Co-Cu system (see appendix C). In (b) and (c), the dashed straight lines indicate the overall trends of the experimental data. The vertical dash-dotted line indicates the critical Cu concentration below which an hcp phase can only be observed and above which an fcc phase also appears. For samples with Cu content above 2.5 at%, the hcp lattice parameters could not be determined due to the large fcc phase fraction.

As discussed in the appendix, a solid solution can form at least in Co-rich Co-Ni alloys in the hcp structure without the necessity of an excess volume due to heat of mixing. This implies that the composition dependence of the lattice constants and the average atomic volume follow Vegard's law. It can be seen in Fig. 8 that the overall trend of the experimental data with composition for the "hcp"-Co(Ni) alloy deposits (see dashed lines drawn parallel to the corresponding Vegard lines) also follow Vegard's law apart from the deviation in the absolute values of the lattice parameters for reasons mentioned above.

The lattice parameter of the fcc phase could be evaluated for three "hcp"-Co(Cu) electrodeposits and these data are displayed in Fig. 9 by using the (200) and (222) XRD peak positions and the Nelson-Riley evaluation method. For reference, the data on melt-quenched (MQ) Co-Cu alloys[18] are also shown which represent the increased lattice parameter due to the excess volume of the alloy formation in the fcc Co-Cu system (see Fig. A·3). One can see in Fig. 9 that the lattice parameter a_{fcc} of the fcc phase in the "hcp"-Co (Cu) electrodeposits mostly follows within error the behavior of the MQ Co-Cu alloys.

According to Table II, for the "hcp"-Co(Ni) electrodeposits a significant fcc fraction was obtained only in the alloy with the highest Ni content (8.5 at%) which was revealed by the appearance of unique fcc peaks with considerable intensity in the diffractogram obtained in BB configuration. These unique fcc peaks were not observed in the PB pattern of the "hcp"-Co(Ni) sample with 8.5 at% Ni. Since the lattice constants for both the hcp and fcc phases were determined from the individual reflections in the PB patterns, therefore the lattice parameter for this material was not calculated.

Magnetoresistance Characteristics

First, we will present the magnetoresistance results for the "hcp"-Co(Cu) series. The MR(H) curves are shown in Fig. 10 for the smallest (EH-01) and largest (EH-13) Cu-contents as well as for sample EH-10 (2.49 at% Cu) which had the smallest Cu content at which a clearly visible fcc phase appeared according to the XRD studies. Although the MR(H) curves appear qualitatively very similar for all compositions, we can still observe two important differences between the hcp samples and the mixed hcp+fcc samples.

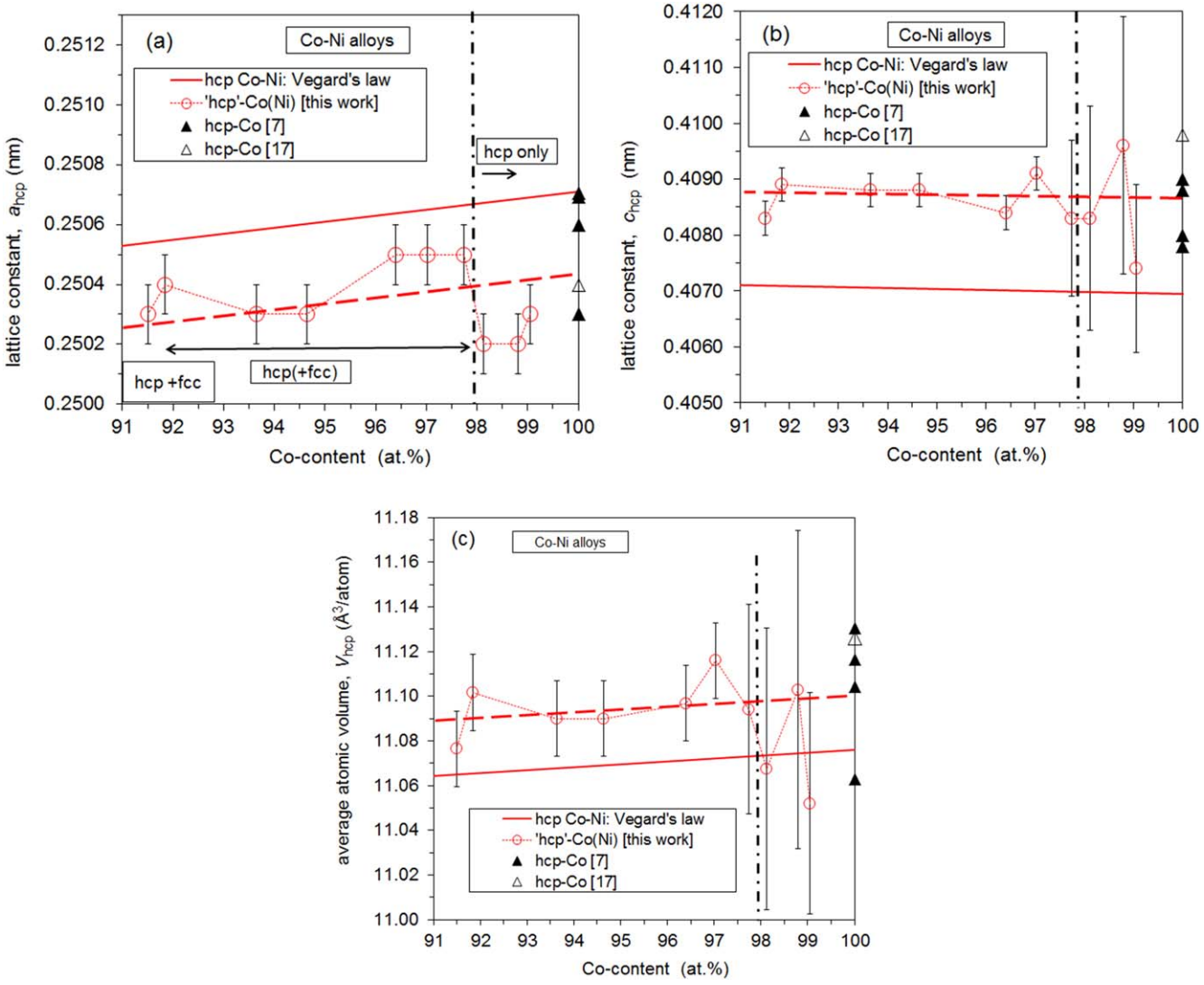

Figure 8. Lattice constants a_{hcp} (a) and c_{hcp} (b) and average atomic volume V_{hcp} (c) of the hcp phase in the "hcp"-Co(Ni) (◯) electrodeposits. Previous results for pure electrodeposited hcp-Co are also added (▲[7] and Δ[17]). The solid line corresponds to Vegard's law for the hcp phase in the Co-Ni system (see Appendix D). The vertical dash-dotted line indicates the critical Ni concentration below which an hcp phase can only be observed and above which an fcc phase also appears. For samples with Ni content between 2 and 8 at%, the fcc phase fraction is minor and above 8 at% is significant.

First, a clear peak narrowing can be observed at the transition from the fully hcp phase to the hcp+fcc phase mixture with increasing Cu content (compare the MR(H) curves for EH-01 and EH-10, upper panels in Fig. 10). A similar difference in the width of the MR(H) curves was seen for the pure Co deposits[7] between the fully hcp and the predominantly fcc samples, the broader MR(H) curves of the hcp-Co phase being caused by the higher magnetocrystalline anisotropy of this phase. In order to illustrate this change for the "hcp"-Co(Cu) series, the lower right panel in Fig. 10 shows a comparison of the LMR(H) curves for the selected three samples (EH-01, EH-10 and EH-13).

Second, one can see that for the fully hcp Co-Cu alloy sample EH-01 (dashed line), the MR(H) curve does not reach saturation up to high magnetic fields, similarly as observed for the pure hcp-Co samples previously.[7] On the other hand, for both samples containing an fcc phase fraction (EH-10 and EH-13), saturation is achieved around 2 to 3 kOe magnetic field above which an approximately linear decrease of the MR(H) curves can be seen. The latter behavior is again similar to the previously studied[7] electrodeposited pure Co samples with predominantly fcc phase.

Since the MR saturation field cannot be unambiguously determined, we have rather used the width of the measured MR(H) curves in order to better characterize the evolution of the magnetoresistance curves with Co content. For this purpose, the half width at half maximum (HWHM) was determined for all the measured MR(H) curves and these data are displayed in Fig. 11.

The situation is clear for the "hcp"-Co(Cu) deposits in that the HWHM values (open and closed diamond symbols) show a continuous decrease (see solid line) starting from pure hcp-Co to the highest Cu content (i.e., the lowest Co content), in agreement with the evolution of the MR(H) curves presented in Fig. 10.

The data in Fig. 11 show that for pure hcp-Co and for hcp Co-Cu alloys with low Cu content (not exceeding about 2 at%), due to the high magnetocrystalline anisotropy of the hcp structure, the approach to saturation of the magnetization and, thus, also the magnetoresistance, requires high magnetic fields. The alloyed small amount of Cu reduces the magnetocrystalline anisotropy of the hcp Co-Cu alloys as evidenced by the decreasing values of HWHM. When the Cu content goes beyond about 2 at%, an fcc phase fraction also appears in the "hcp"-Co(Cu) deposits which phase is characterized by much smaller magnetocrystalline anisotropy and, therefore, the HWHM further reduces to values which are close to the HWHM value obtained for the predominantly fcc phase samples of pure Co

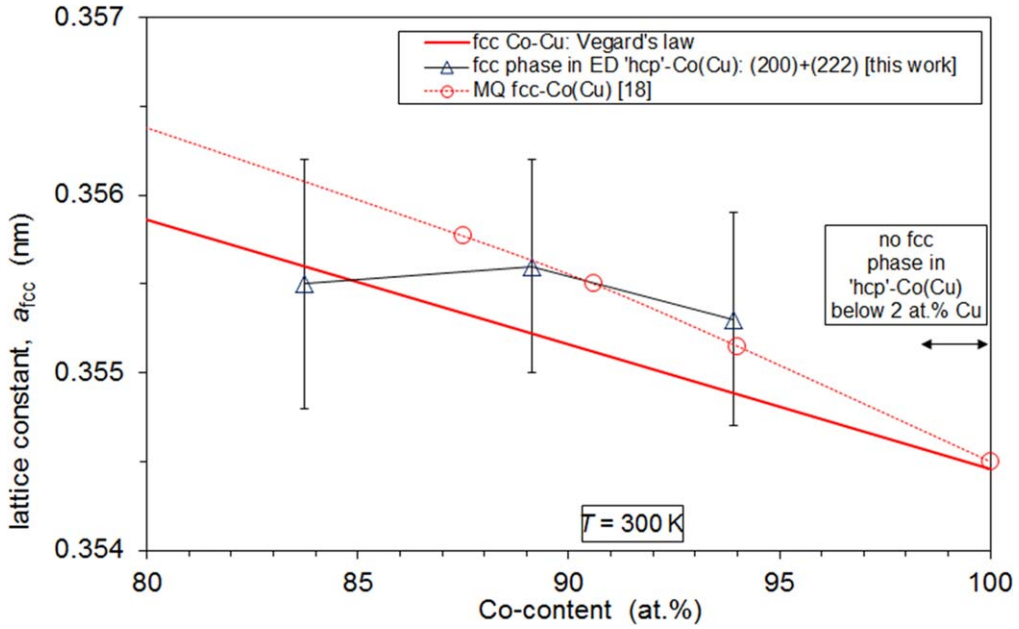

Figure 9. Lattice constant a_{fcc} of the fcc phase in those "hcp"-Co(Cu) electrodeposits for which the structural parameters of the fcc phase could be evaluated besides the major hcp phase. The solid line corresponds to Vegard's law for the fcc phase in the Co-Cu system (see appendix E). The red open circles (◯) represent the data of Klement[18] on melt-quenched (MQ) fcc Co-Cu alloys.

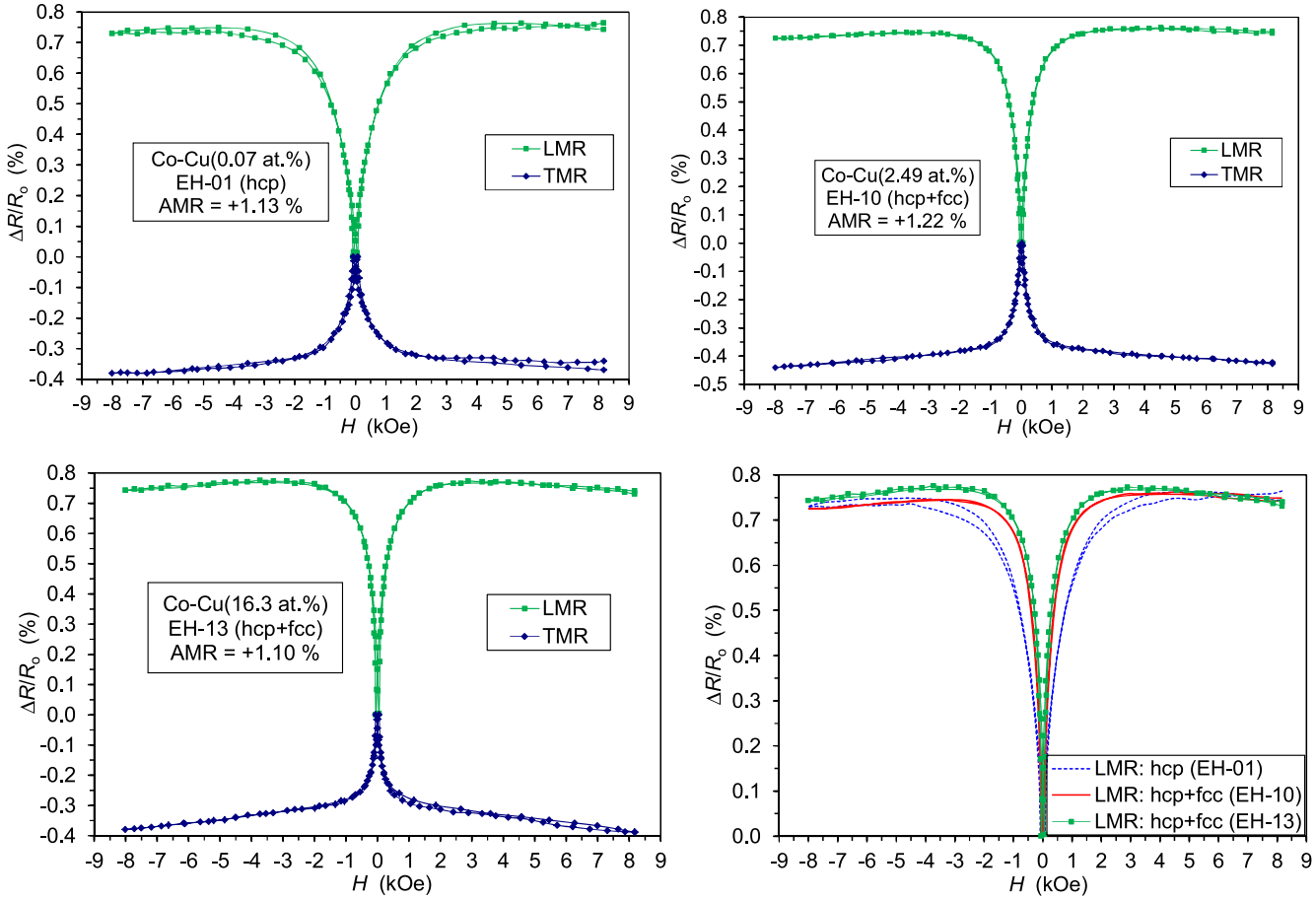

Figure 10. Longitudinal and transverse MR(H) curves (labelled as LMR and TMR, respectively) for the smallest (EH-01) and largest (EH-13) Cu contents as well as for sample EH-10 (2.49 at% Cu) for which clear fcc peaks first appear in the XRD patterns. The right lower panel displays the longitudinal MR(H) curves for these three samples on a common plot.

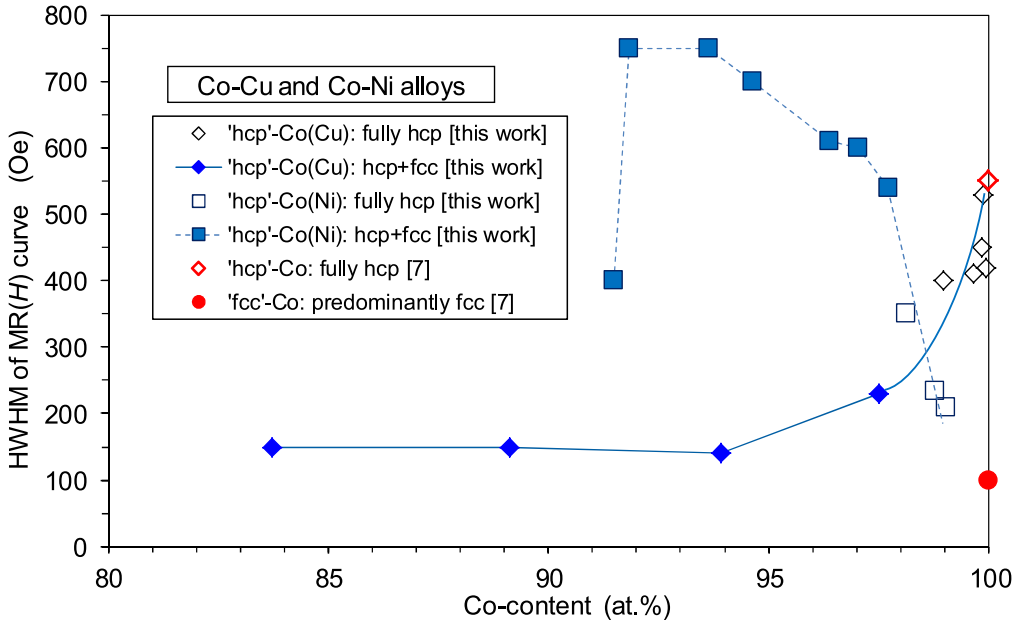

Figure 11. Half width at half maximum (HWHM) of the MR(H) curves as a function of the Co content for the "hcp"-Co(Cu) and "hcp"-Co(Ni) deposits. The solid (Co-Cu) and dashed (Co-Ni) lines are intended only to show the overall evolution of the data with composition. The values for the pure hcp-Co phase and for the predominantly fcc-Co phase samples are also indicated from our previous work.[7]

deposits reported in our previous work[7] as indicated by the full circle in Fig. 11.

The MR(*H*) curves of the "hcp"-Co(Ni) alloy deposits were qualitatively very similar to those of the "hcp"-Co(Cu) deposits shown in Fig. 10. However, the Co-Ni alloy deposits consisting of a hcp phase only (i.e., having a Ni content below about 2 at%) exhibited fairly narrow MR(*H*) curves with low saturation fields and with a linearly decreasing high-field range. On the other hand, when the overall Ni content exceeded about 2 at% where the deposits contained besides the main hcp phase also a very small fcc phase fraction, the peak of the MR(*H*) curves broadened and the saturation field increased. Finally, in the deposit with the highest Ni content in which a significant fcc fraction was already present, the MR(H) curves became again fairly narrow. All these features are reflected in the evolution of the HWHM values with Co content as demonstrated in Fig. 11 by the open and closed data points connected by a dashed line.

In contrast to the Co-Cu system, it is not easy to rationalize the observed variation of the HWHM values with composition in the Co-Ni system. Surprisingly, although the three samples with the lowest Ni content still consist of an hcp phase only, the HWHM values which are only about half of the corresponding parameter of the pure hcp-Co phase[7] indicate a magnetic softening. This implies as if the addition of Ni in such a small amount to the hcp phase of Co would reduce the magnetocrystalline anisotropy. The situation is further complicated by the fact that after the initial reduction, the HWHM values continuously increase upon the addition of more and more Ni to the hcp lattice in spite of the fact that also the magnetically softer fcc phase appears in the samples. As a possible cause of this peculiar behavior, we might invoke for a non-monotonic change of the crystallographic texture when increasing the amount of added Ni in the hcp lattice. Namely, according to our previous work on pure hcp-Co electrodeposits,[7] the magnetic easy axis (*c*-axis) was found to lie in the deposit plane. It was demonstrated there that this feature leads to lower saturation fields in the deposit plane than reported for metallurgically processed bulk polycrystalline hcp-Co samples. This implies that the actual texture of the hcp phase may have a strong influence on the final resulting saturation behavior of polycrystalline hcp-Co samples. The strong reduction of HWHM for the Co-Ni sample with the highest Ni content may be explained by recalling (cf Fig. 5) that in this sample the fcc phase fraction becomes suddenly almost comparable to the hcp fraction.

There is indeed a strong texture variation with increasing Ni content in the "hcp"-Co(Ni) electrodeposits as demonstrated by the XRD patterns measured in PB diffraction configuration and shown in Fig. 12. We can see that for sample MH-3 having only an hcp phase, the hcp $(10\bar{1}0)$ peak has a much higher intensity than the hcp $(10\bar{1}1)$ peak (samples MH-1 and MH-2 exhibited a similar XRD pattern). Increasing slightly the Ni content (MH-4), the intensity of the hcp $(10\bar{1}1)$ peak becomes almost comparable to that of the hcp $(10\bar{1}0)$ peak. Although for higher Ni contents the relative intensity of the hcp $(10\bar{1}1)$ peak gradually decreases with respect to the hcp $(10\bar{1}0)$ peak, we can still see a sudden return to the original intensity ratio between the two samples with the highest Ni contents (from sample MH-9 to sample MH-11). The texture change is certainly induced by the appearance of the fcc phase (first in sample MH-4) and the continuous increase of its fraction in the samples (cf Fig. 5), especially the abrupt increase of the fcc fraction in sample MH-11. These texture variations support the considerations put forward in the previous paragraph in an effort to explain the non-linear variation of the HWHM values with composition in the "hcp"-Co(Ni) electrodeposits. It may also be noted here that no texture evolution with Cu content could be observed for the "hcp"-Co(Cu) electrodeposits.

Another parameter characterizing the magnetization/magnetoresistance reversal behavior is the coercive field (H_c) and the peak position H_p of the magnetoresistance curves. As discussed elsewhere,[19] the values of the two quantities are close to each other, but should not be necessarily equal. Nevertheless, it may be useful to compare the composition dependence of parameter H_p for the Co-Cu and Co-Ni alloy deposits (Fig. 13) with the HWHM data. One should keep, however, in mind that both H_p and H_c are strongly microstructure-dependent parameters, i.e., they depend on, e.g., the grain size which, on the other hand, may vary with composition and type of alloying element added to the matrix metal.

Nevertheless, the H_p values for the pure hcp phase samples both for the Co-Cu and the Co-Ni systems are at least as high as for the pure hcp-Co phase which is appropriate. The H_p values for the mixed phase samples of the Co-Ni system are similarly high and this matches the high HWHM values for this system. The H_p values for

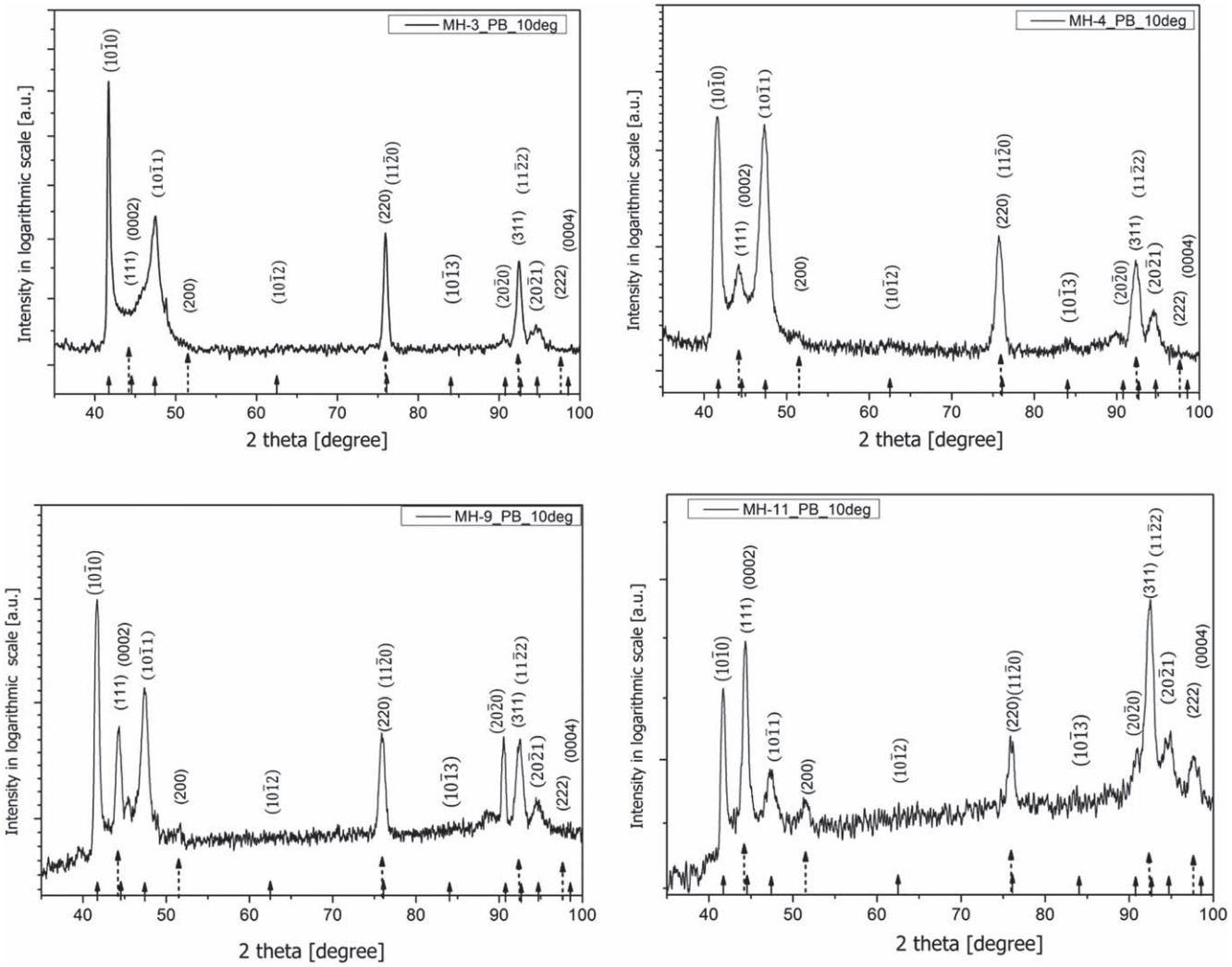

Figure 12. XRD patterns measured in the PB geometry for "hcp"-Co(Ni) electrodeposits: sample MH-3 (1.88 at% Ni; upper left panel), MH-4 (2.27 at% Ni; upper right panel), MH-9 (8.16 at% Ni; lower left panel) and sample MH-11 (8.5 at% Ni; lower right panel).

the mixed phase samples of the Co-Cu system are lower than for the Co-Ni system, they are intermediate between the values for the pure hcp-Co and predominantly fcc-Co samples and to some extent corresponding to the HWHM values of the Co-Cu system. Overall, there is some proper correspondence between the HWHM and H_p values, both parameters characterizing, to some degree, the magnetic softness.

The AMR ratio was not found to change significantly throughout the Co-Cu series as Fig. 14 shows. In spite of the large AMR ratio of the pure fcc-Co phase,[7] the AMR ratios of the mixed hcp+fcc samples remain for all "hcp"-Co(Cu) deposits around the pure hcp-Co value.[7] With increasing Cu content, the fraction of the fcc phase having a higher AMR ratio increases, so one could expect an increase of the AMR ratio. However, an increasing amount of Cu in either the hcp or the fcc Co-Cu phases may induce changes in the electronic density of states around the Fermi level to cause a decrease of the AMR ratio. The two effects may counteract, resulting in the observed nearly constant behavior of the AMR ratio as a function of the Cu content.

Figure 15 shows that the AMR ratio increases nearly monotonically in the "hcp"-Co(Ni) deposits from the pure hcp-Co value with increasing Ni content. This may occur for two reasons: first, the AMR increases with Ni content also for the fcc phase as the literature data in Fig. 15 indicate and, second, with increasing overall Ni content, the amount of the fcc phase also increases and the fcc phase has a higher AMR ratio, almost by a factor of 2 than the hcp phase.[7]

Summary

In this work, Co-Cu and Co-Ni alloy electrodeposits were prepared under conditions which proved to yield fully hcp-Co phase from a sulfate type bath[7] and their structure and magnetoresistance (MR) characteristics were investigated. The alloying element incorporation was achieved by adding varying amounts of $CuSO_4$ and $NiSO_4$, respectively, to the $CoSO_4$ bath. The primary interest of the present study was to establish the amount of Cu and Ni which can be accommodated in the hcp-Co lattice in these nanocrystalline deposits.

First, a detailed structural study by various X-ray diffraction (XRD) geometries was carried out. In both the Co-Cu and Co-Ni systems, an hcp phase was only formed up to about 2 at% of the alloying element. Above this concentration, a significant amount of fcc phase appeared in Co-Cu and a minor fcc fraction in Co-Ni up to about 8 at%. This means that in these nanocrystalline deposits, hcp-Co could dissolve about 2 at% Cu and at least about 8 at% Ni in its lattice without the formation of a considerable fraction of the fcc phase.

It was obtained for the Co-Ni system that both hcp lattice parameters (and also the average atomic volume) exhibits an

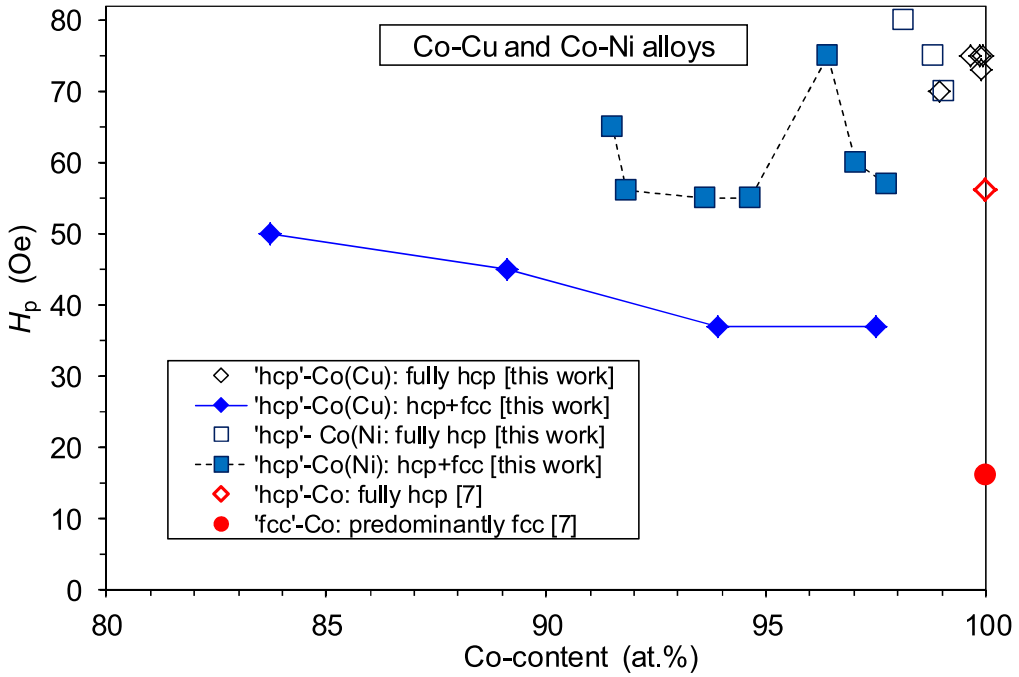

Figure 13. Magnetoresistance hysteresis parameter *H*p as a function of the Co content for the "hcp"-Co(Cu) and "hcp"-Co(Ni) deposits. The values for the pure hcp-Co phase and the for the predominantly fcc-Co phase samples are also indicated from our previous work.[7]

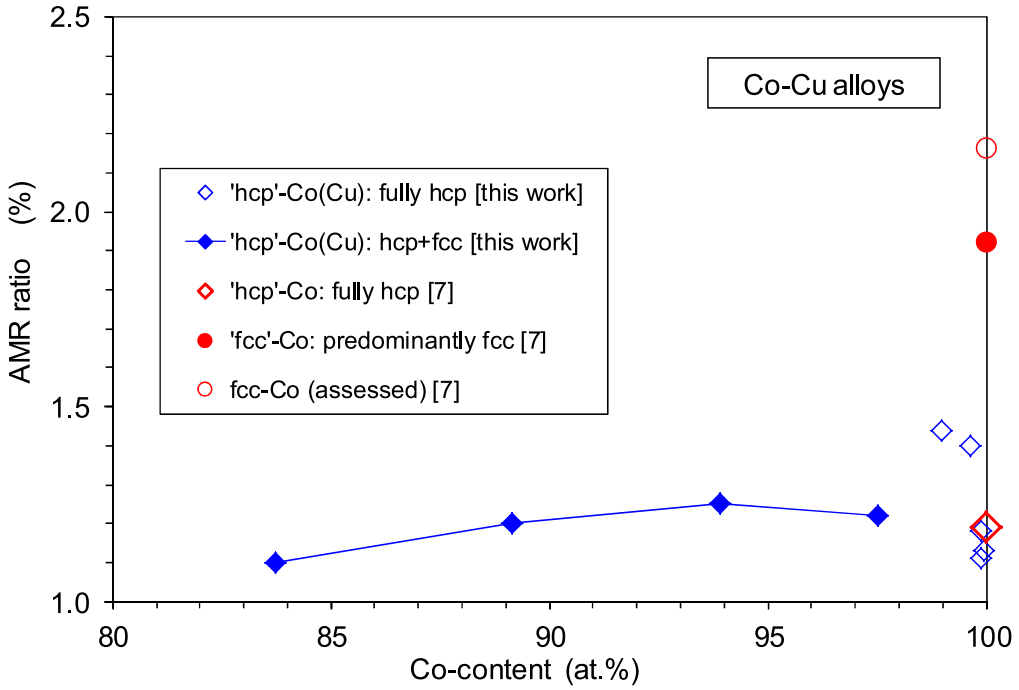

Figure 14. AMR ratio as a function of the Co content for the "hcp"-Co(Cu) deposits. The values for the pure hcp-Co and fcc-Co phases and for the predominantly fcc-Co phase samples are also indicated from our previous work.[7]

approximately linear decrease with increasing Ni content. This indicates that the hcp-Co lattice can accommodate the smaller Ni atoms with a slight contraction of the lattice. This is in agreement with our other observation that up to about 8 at% Ni an hcp phase is dominating with a very small fcc fraction only, i.e., the Ni atoms incorporated in the deposits are predominantly in the hcp phase. The variation of the lattice parameters and the average atomic volume with Ni content was found to correspond approximately to Vegard's law due to the miscibility of Co and Ni in the hcp phase for Co-rich Co-Ni alloys.

The hcp lattice parameters of the Co-Cu deposits showed an increase with the addition of Cu atoms and the increase was stronger than the change according to the Vegard's law. The same was found also for the average atomic volume. This behavior is in agreement with literature results on fcc Co-Cu alloys in that this latter system also exhibited a positive deviation from Vegard's law due to the excess volume required for the formation of the non-equilibrium fcc phase. Our present results, as well as other reported data shown in Appendix E (Fig. A·6), indicate that the excess volume for alloy formation in the Co-Cu system is required also in the case of the hcp phase.

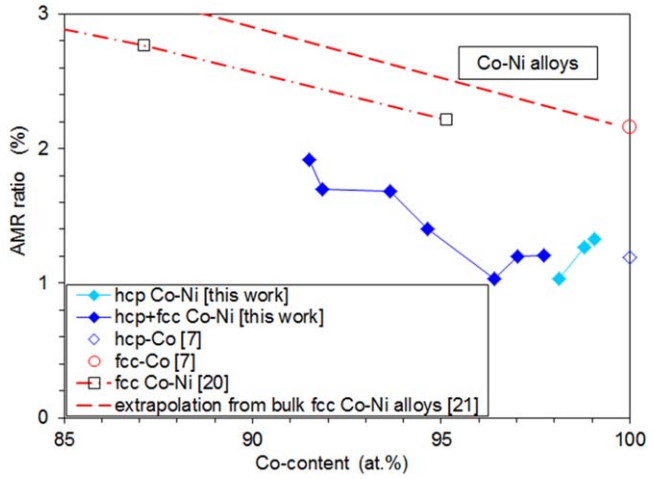

Figure 15. AMR ratio as a function of the Co content for the "hcp"-Co(Ni) deposits. Previous data for the pure hcp-Co and fcc-Co phases[7] and for predominantly fcc Co-Ni alloys[20] are also displayed. The dashed line indicates an extrapolation from our unpublished work[21] for fcc Co-Ni alloys.

All deposits exhibited the usual AMR phenomenon in that the magnetoresistance was positive for the LMR configuration and negative for the TMR configuration. For low alloying element concentrations, i.e., for the hcp alloy phases, the AMR ratio was found for both alloy systems to be close to the pure hcp-Co value reported previously.[7] For the Co-Cu system, a slight decrease of the AMR ratio was observed with increasing Cu concentration as a consequence of the changes in the electronic density of states due to the alloyed non-magnetic Cu in the ferromagnetic Co matrix. For the hcp Co-Ni alloys, the AMR ratio showed a slight increase with increasing Ni-content. This is in agreement with previous results[20,21] according to which the maximum AMR ratio in the Co-Ni system is around 75 at% Ni.

Acknowledgments

Funding: The Wigner Research Centre for Physics utilizes the research infrastructure of the Hungarian Academy of Sciences and is operated by the Eötvös Loránd Research Network (ELKH) Secretariat (Hungary). M. El-Tahawy acknowledges the support of the Egyptian Government by providing a postdoc fellowship to the Eötvös Loránd University, Budapest, Hungary.

Data Availability Statement

The data that support the findings of this study are available from the authors upon reasonable request.

Author Contributions

Conceptualization, L.P. and I.B.; methodology, M.E.T and L.P.; formal analysis, M.E.T; investigation, L.P. and M.E.T.; resources, L. P., G.M. and J.G.; writing—original draft preparation, I.B. and M.E. T; writing—review and editing, I.B., L.P., J.G. and L.V.; theoretical calculations, C.L. All authors have read and agreed to the published version of the manuscript.

Appendix

A. On the composition dependence of the lattice parameters and average atomic volume in random binary alloys.—In an ideal substitutional solid solution, the constituent atoms are randomly distributed on the lattice sites and the thermodynamic excess properties of mixing are zero (e.g., there is no excess volume due to mixing and there is no excess heat of mixing). Therefore, the molar volume and the unit cell volume (or, equivalently, the average atomic volume) are linear functions of the composition or mole fraction.

This behavior was noted for the first time by Retgers[22] as early as in 1889 and has been frequently discussed since then even until quite recently,[23–26] mentioning it sometimes as Retgers' law.[25] For an ideal binary solid solution alloy $A_{1-x}B_x$, the depicted linear variation of the average atomic volume $V_{A\text{-}B}$ can be represented as a linear composition-weighted sum of the atomic volumes V_A and V_B of the constituents:

$$V_{A-B} = (1 - x)V_A + xV_B \qquad [A\cdot1]$$

where $0 \leqslant x \leqslant 1$ is the molar fraction of component B. As a specific example of such a behavior, the amorphous $Zr_{1-x}Cu_x$ alloy system can be mentioned. It turned out from an analysis of average atomic volume data[2] derived from reported density values that (i) the $V_{Zr\text{-}Cu}$ data decrease linearly with increasing Cu content and (ii) these data can be fitted by a straight line intersecting the ordinate axis at V_{Zr} at $x = 0$ and at V_{Cu} at $x = 1$. This just means that for the amorphous Zr-Cu alloys, Eq. (A·1) can be applied, i.e., these alloys behave as an ideal solid solution. The randomness manifests itself in the fact that there is no chemical short-range order which means that the average composition of the first-neighbor coordination shell of any of the constituent atoms corresponds to the overall chemical composition of the particular alloy under consideration.

In non-ideal solid solutions, an excess volume term also enters and, instead of Eq. 1, we have

$$V_{A-B} = (1 - x)V_A + xV_B + \Delta V_m(x) \qquad [A\cdot2]$$

where the composition dependent term $\Delta V_m(x)$ is the change in average atomic volume due to alloy formation, which in thermodynamics often goes by the name of volume of mixing (therefore, the subscript m refers to mixing). In such cases, evidently, the linear composition dependence of the atomic volume is no more valid. The metastable face-centered cubic (fcc) Co-Cu system is an example of a non-ideal solid solution alloy series in which, due to the positive heat of mixing, alloy formation is accompanied by an increase of the average atomic volume.[27,28] We will later demonstrate this behavior of the Co-Cu system.

About a century ago, Vegard[29] noticed that in some disordered binary crystalline mixtures, the lattice parameter changes linearly with the fractions of the two components. For a binary fcc alloy system with the lattice parameter $a_{A\text{-}B}$, this corresponds actually to a relation analogous to Eq. (A·1), namely

$$a_{A-B} = (1 - x)a_A + x\,a_B \qquad [A\cdot3]$$

where a_A and a_B are the lattice constants of the pure constituents. This so-called Vegard's law became very popular in crystallography and materials science[23–26] for analyzing the composition variation of the lattice parameter of any binary alloys with various crystal structures. It was noticed, however, already a long time ago by Zen[23] that even if the average atomic volume of an alloy system obeys Retgers' law, due to the relation between lattice parameter(s) and the average atomic volume (e.g., for a face-centered cubic (fcc) structure: $V_{fcc} = a^3/4$, for a hexagonal close-packed (hcp) structure $V_{hcp} = \sqrt{3}\,a^2c/4$ where a and c are the lattice constants of the hcp structure and for a body-centered cubic (bcc) structure $V_{bcc} = a^3/2$), Vegard's law is only an approximation. Therefore, a linear variation of the lattice parameter with composition occurs, i.e., Vegard's law is obeyed, only if the relative difference of the lattice parameters of the two constituents is much smaller than unity. More recently, Jacob et al.[24] has made a more quantitative analysis about the validity of Vegard's law. They demonstrated for the case of an fcc structure that Vegard's law is obeyed, i.e., the deviation of the composition dependence of the lattice parameters from Vegard's law is negligible, for those binary alloy systems in which the relative

difference of the lattice parameters of the constituents does not exceed about 5%. For random solid solutions, this upper limit may probably apply also for non-cubic structures. At the same time, this also means that if the relative difference of the lattice parameters is smaller than 5%, both Retgers' law and Vegard's law are obeyed simultaneously.

In the present paper, we are interested in the Co-Cu and Co-Ni alloy systems. Therefore, we summarize available experimental and theoretical data on the lattice parameters of the fcc and hcp phases of the three metals as well as their variation with composition in the two binary systems. As we will see, the lattice parameter differences for the Co-Cu and Co-Ni systems remain well below the 5% threshold. Therefore, for the sake of simplicity, we will call also the linear composition dependence of the average atomic volume as Vegard's law.

B. Experimental lattice parameters and average atomic volumes of the fcc and hcp phases of Co, Cu and Ni metals at room temperature.—In view of the very careful data evaluation procedure by Vincent and Figlarz,[16] their room-temperature result $a_{\text{fcc-Co}} = 0.35446(1)$ nm is considered to be a reliable value for the metastable fcc-Co phase which is also quoted in the crystallographic data reference work of Villars and Calvert.[30] Within error, a very similar value ($a_{\text{fcc-Co}} = 0.35447$ nm) was reported by Swanson et al.[31] which is quoted in one of the standard ASTM Powder Diffraction Files.[13] From the lattice parameter of Vincent and Figlarz,[16] the average atomic volume is obtained as $V_{\text{fcc-Co}} = 11.13$ Å^3/atom.

The lattice parameter of the stable fcc-Cu and fcc-Ni phases is also taken from the reference work of Villars and Calvert:[30] $a_{\text{fcc-Cu}} = 0.36148$ nm which yields $V_{\text{fcc-Cu}} = 11.81$ Å^3/atom and $a_{\text{fcc-Ni}} = 0.35232$ nm which yields $V_{\text{fcc-Ni}} = 10.93$ Å^3/atom.

One can see from these data, that the relative fcc lattice parameter difference for the Co-Cu system is $\Delta a/a = 1.98\%$ and for the Co-Ni system is $\Delta a/a = 0.61\%$. This means that, according to the considerations of Jacob et al.,[24] the lattice parameter variation with composition could obey Vegard's law for equilibrium (stable) phases in both alloy systems. Since Co and Ni can form continuous solid solutions for all compositions in the fcc phase,[1] a linear variation of both the average atomic volume and the lattice parameter can be expected for fcc Co-Ni alloys. However, it was noted already above that at room temperature the fcc Co-Cu solid solution system is metastable with an additional volume of mixing upon alloy formation, so neither the average atomic volume nor the lattice parameter are expected to vary linearly with composition as will be shown later.

The stable phase of Co at room temperature is the hcp structure and several experimental lattice parameter sets are collected in the reference works of Villars and Calvert.[30,32] Similarly to fcc-Co, we prefer also for hcp-Co the values of Vincent and Figlarz[16] since these authors have performed a very careful deduction of the lattice parameters from their experimental data and their values are $a_{\text{hcp-Co}} = 0.25071(3)$ nm, $c_{\text{hcp-Co}} = 0.40695(5)$. From these values, one gets the average atomic volume $V_{\text{hcp-Co}} = 11.08$ Å^3/atom which is close to $V_{\text{fcc-Co}} = 11.13$ Å^3/atom. The small difference (ca. 0.5%) of the two atomic volumes is actually expected since both phases exhibit a close-packed structure. The derived axial ratio of hcp-Co from the data of Vincent and Figlarz[16] is $c/a = 1.623$ which is close to the value $c/a = \sqrt{(8/3)} = 1.633$ for hexagonal closest packing of spheres.[33]

The only report on the metastable hcp-Cu phase is the work of Takahashi[34] who investigated electrodeposited thin Cu films by electron diffraction and obtained $a_{\text{hcp-Cu}} = 0.2551$ nm. He assumed the ideal axial ratio for a hcp crystal ($c/a = 1.633$) from which the value $c_{\text{hcp-Cu}} = 0.4166$ nm and an average atomic volume $V_{\text{hcp-Cu}} = 11.74$ Å^3/atom can be derived. We can check the reliability of these data in different ways. First, both lattice parameters are larger by roughly the same factors for Cu than those for Co, in agreement with the known larger size of Cu atoms than Co atoms. Second, the average atomic volume of $V_{\text{hcp-Cu}}$ is by only less than 1% different from the standard value for fcc-Cu ($V_{\text{fcc-Cu}} = 11.81$ Å^3/atom[30]) and such a small difference is expected due to the close-packed structure of both phases. Third, a comparison of the differences between the average atomic volumes of the two phases for both Co and Cu shows a similarly good matching. Namely, the atomic volume increment from Co to Cu is $V_{\text{hcp-Cu}}—V_{\text{hcp-Co}} = 0.66$ Å^3/atom for the hcp phase and $V_{\text{fcc-Cu}}—V_{\text{fcc-Co}} = 0.68$ Å^3/atom for the fcc phase. This means that on the basis of the data of Takahashi,[34] the lattice expansion of hcp-Cu with respect to the standard hcp-Co data[12] is just as expected. Fourth, according to the considerations of Wright and Goddard[35] on the basis of the matching of certain lattice planes of the hcp and fcc structures, the expected value of a_{hcp} of a given element may be estimated from a_{fcc} of the same element via the formula $a_{\text{hcp}} = a_{\text{fcc}}/\sqrt{2}$. By using the standard value $a_{\text{fcc-Cu}} = 0.36148$ nm,[30] it can be expected that $a_{\text{hcp-Cu}} = 0.2556$ nm and the experimental value ($a_{\text{hcp-Cu}} = 0.2551$ nm[34]) is fairly close to this expected value.

It is noted that if we take the value $c/a = 1.623$ obtained experimentally above for hcp-Co and use it for the calculation of $c_{\text{hcp-Cu}}$, then we get $c_{\text{hcp-Cu}} = 0.4140$ nm from the experimental value $a_{\text{hcp-Cu}} = 0.2551$ nm of Takahashi[34] which differs by about 0.5% only from the value $c_{\text{hcp-Cu}} = 0.4166$ nm derived with the ideal value $c/a = 1.633$. Similarly, the average atomic volumes obtained by the two different axial ratios differ by less than 1%. Anyway, these differences will be really negligible for Co-rich alloys in which we are mainly interested from the viewpoint of our experimental results.

It follows from the above data that when going from pure hcp-Co to pure hcp-Cu, a_{hcp} increases by about 2%, c_{hcp} increases by 2.36% and V_{hcp} increases by about 6%.

There are numerous structural reports for the metastable hcp-Ni phase from which we will select the reliable ones mainly on the basis of the average atomic volume $V_{\text{hcp-Ni}}$ that can be derived from the reported lattice constants $a_{\text{hcp-Ni}}$ and $c_{\text{hcp-Ni}}$.

For getting reliable values for the lattice constants of hcp-Ni, we will proceed as follows. Table A·I lists those works in which the reported lattice constant data result in a $V_{\text{hcp-Ni}}$ value which differs by less than 2% from the standard $V_{\text{fcc-Ni}}$ value. This corresponds to the constraint that, as we could see for Co and Cu, the average atomic volumes of the two close-packed structure of Ni must not differ significantly. The last row of this table gives the average values for hcp Ni: $a_{\text{hcp-Ni}} = 0.2487$ nm and $c_{\text{hcp-Ni}} = 0.4087$ nm from which the average atomic volume is $V_{\text{hcp-Ni}} = 10.95$ Å^3/atom, in very good agreement with $V_{\text{fcc-Ni}} = 10.94$ Å^3/atom.

There are numerous further structural studies on the metastable hcp-Ni phase, which are not listed here, because these studies reported lattice constants yielding an average atomic volume $V_{\text{hcp-Ni}}$ differing by more than 2% from the standard $V_{\text{fcc-Ni}}$ value (in several cases the deviation amounting to as high as 15 to 20%).

It follows from the above data that when going from pure hcp-Co to pure hcp-Ni, a_{hcp} decreases by 0.7%, c_{hcp} increases by 0.4% and V_{hcp} decreases by 1%. One can see that the relative change of the lattice constants and the average atomic volume is much smaller in the Co-Ni system than in the Co-Cu system, simply due to the larger size of Cu atoms in comparison with both Co and Ni.

The data in this section demonstrated that, for both the hcp and fcc phases, the lattice parameter differences between Co and Cu as well as between Co and Ni are small enough so that if the alloy formation in the Co-Cu and Co-Ni systems enables the validity of Retgers' law, then the validity of Vegard's law is also fulfilled.

C. Composition dependence of the lattice parameters for hcp Co-Cu alloys.—Based on the experimental lattice parameter data summarized in appendix B, we have constructed Vegard's law plots for the hcp Co-Cu system in Fig. A·1 in which the solid lines show the composition dependence of the lattice parameters and the average atomic volume.

The only available previous experimental structural report on the hcp Co-Cu system is the work of Shimizu et al.[40] on electrodeposited Co-Cu alloys which contained both hcp and fcc phases. Their

Table A·I. Experimental lattice constants, axial ratios and average atomic volumes reported for the hcp-Ni phase. Included are only those reports for which the difference ΔV(fcc-hcp) = ($V_{\text{fcc-Ni}}$ - $V_{\text{hcp-Ni}}$)/$V_{\text{hcp-Ni}}$ is less than 2%. In the last row, the bold values give the average values on the basis of these reports.

hcp-Ni phase	$a_{\text{hcp-Ni}}$ (nm)	$c_{\text{hcp-Ni}}$ (nm)	c/a	$V_{\text{hcp-Ni}}$ (Å^3/atom)	ΔV(fcc-hcp) (%)	References
electrodeposited epitaxial film on Cu single crystal	0.2500	0.3980	1.592	10.77	1.57	35
evaporated epitaxial nanosized islands on MgO single crystal	0.2440	0.422	1.730	10.88	0.56	36
nanoparticles	0.2493	0.4084	1.638	10.99	−0.46	37
water-quenched sintered bulk pellets	0.2506	0.4074	1.626	11.08	−1.25	38
nanoparticles	0.2496	0.4078	1.634	11.00	−0.56	39
average	**0.2487**	**0.4087**	**1.643**	**10.95**	**−0.06**	

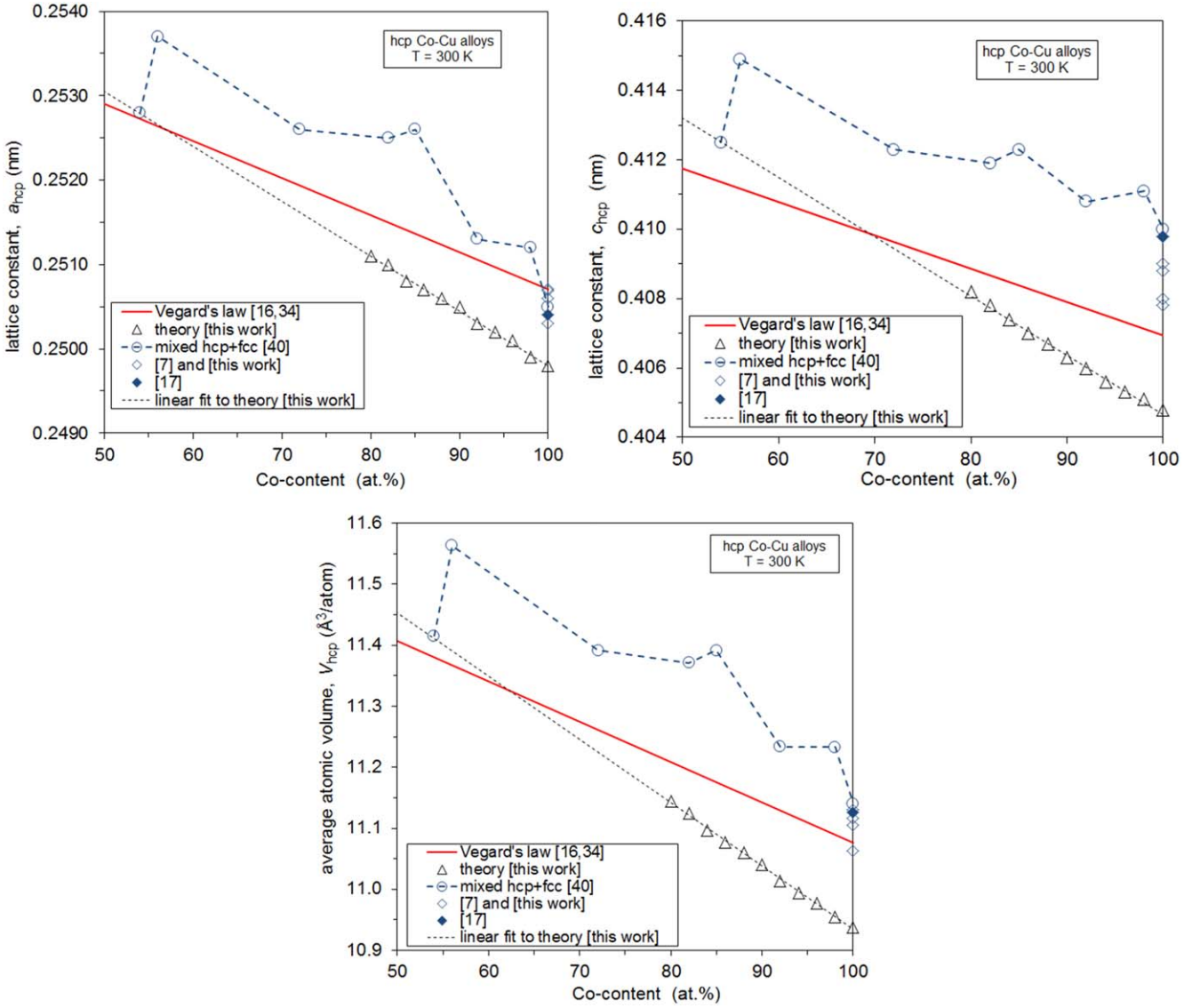

Figure A·1. Composition dependence of the lattice constants a_{hcp} (upper left panel) and c_{hcp} (upper right panel) as well as the average atomic volume V_{hcp} (lower panel) for hcp Co-Cu alloys. The solid line corresponds to Vegard's law for the hcp phase in the Co-Cu system. The open triangles represent our theoretical results for Co-rich alloys and the thin dashed line is a linear fit to these data. The open circles are the experimental results of Shimizu et al.[40] on the hcp phase in electrodeposited Co-Cu alloys containing both hcp and fcc phases. The diamond symbols represent data for electrodeposited hcp-Co from the references indicated.

structural data were obtained by electron diffraction, with most data points lying rather randomly above the Vegard's line as shown in Fig. A·1. In lack of detailed information about the samples and the experimental error of the lattice constants, we cannot further assess these results here. However, we will comment on them in Appendix E after discussing the lattice parameters of fcc Co-Cu alloys.

We have displayed in Fig. A·1 also some data on electrodeposited hcp-Co from Refs. 7 and 17 as well as current measurements for two further samples of Ref. 7 (samples 31 and 37). One can observe that the a_{hcp} and c_{hcp} data for most of the electrodeposited hcp-Co samples fall typically below and above the selected standard value,[16] respectively (due to the different direction of the deviation of the two lattice parameters, the deviation of the corresponding V_{hcp} values appears smaller). These deviations can be explained in the following manner. The electrodeposited samples typically have a relatively small crystallite size and they usually also have some degree of texture. Therefore, a few peaks can only be observed in their XRD patterns and the lattice parameter evaluation should be performed from this low number of peak positions. On the other hand, when Vincent and Figlarz[16] determined the lattice parameters of hcp-Co, their metallurgically prepared bulk samples exhibited a much larger number of diffraction peaks. Therefore, they were able to carry out a systematic correction of their data until reaching a good convergence of all involved peaks. It can be seen from their sketch of the data evaluation procedure that the first step based on a few peaks resulted in systematically smaller value for a_{hcp} and larger for c_{hcp} than the final convergent value when all XRD peaks could already be included in the evaluation. This just corresponds to the cases we can observe for the a_{hcp} and c_{hcp} data of the electrodeposited hcp-Co samples.

Recently, Li et al.[41] have calculated the composition dependence of the lattice constant of chemically disordered (fully random) Co-Cu alloys in the fcc structure by using various ab-initio approaches. We have now calculated similarly the lattice constants for disordered hcp Co-Cu alloys in the composition range 80 to 100 at % Co. All total energy calculations were performed using density functional theory (DFT) in combination with the exact muffin-tin orbital (EMTO) method, Green function and the full charge density techniques. The self-consistent calculations were carried out with the generalized gradient approximation (GGA) via the Perdew-Burke-Ernzerhof (PBE) approximation for describing the exchange-

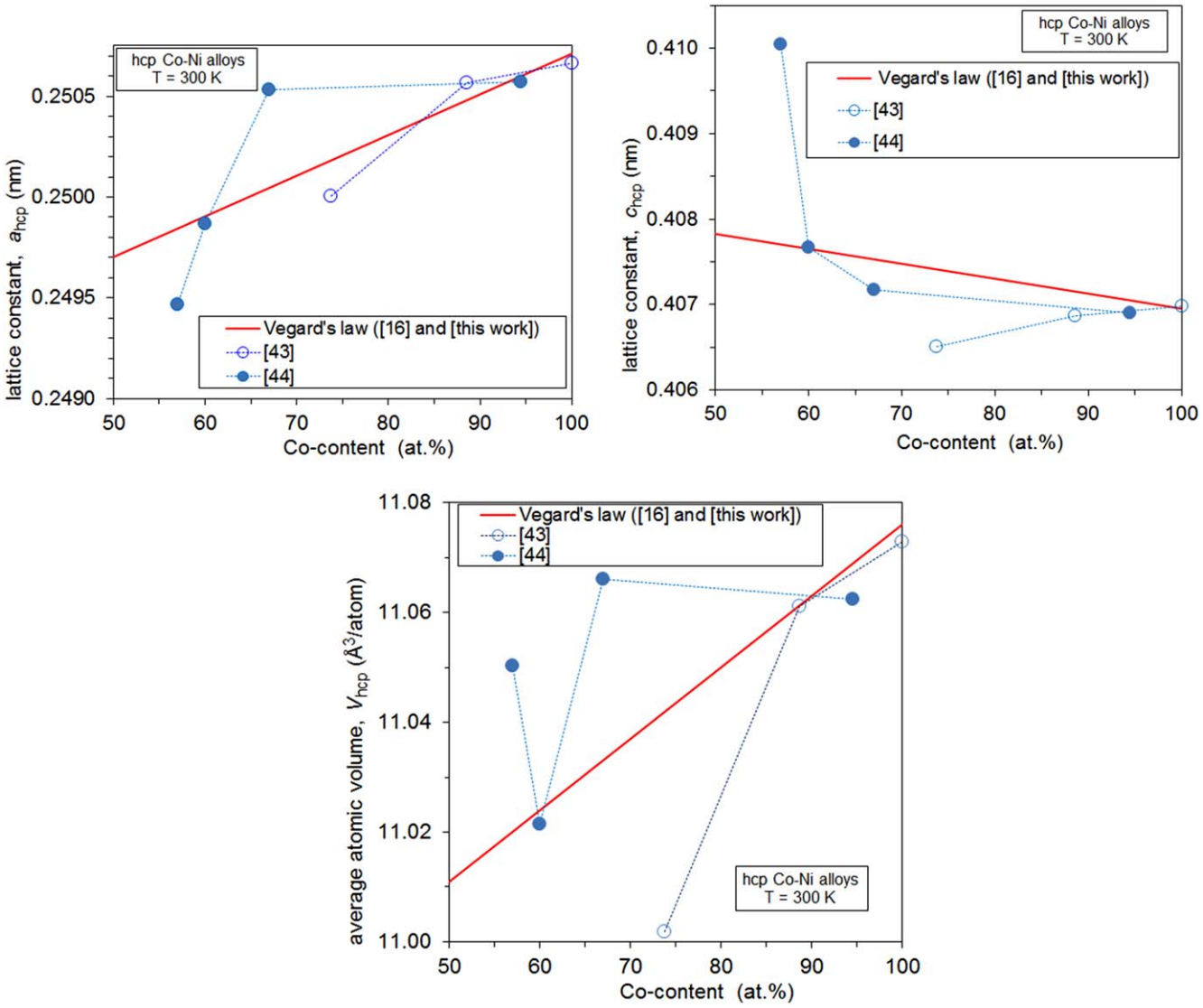

Figure A·2. Composition dependence of the lattice constants a_{hcp} (upper left panel) and c_{hcp} (upper right panel) as well as the average atomic volume V_{hcp} (lower panel) for Co-rich hcp Co-Ni alloys. The solid line corresponds to Vegard's law for the hcp phase in the Co-Ni system. The open circles represent the experimental data of Taylor[43] on metallurgically processed samples. The solid circles are the experimental results of Rafailovic et al.[44] on electrodeposited Co-Ni alloys (specified errors for both lattice constants: ±0.0003 nm).

correlation interactions. The coherent potential approximation (CPA) was adopted to describe the compositional and magnetic disorder. All calculations are treated at the ferromagnetic state due to the high concentration of magnetic Co. A k-point mesh of 29*29*29 was employed in the irreducible Brillouin zone.

The theoretical lattice constants obtained in the above manner are indicated in Fig. A·1 by the open triangles. The theoretical values are very close to the experimental Vegard's line. However, the slope is definitely larger than for the Vegard's line. Both calculated lattice constants underestimate the experimental values by about 0.5% for hcp-Co and their extrapolation to hcp-Cu (dashed line) overestimates the experimental values to a similar extent (by 0.5% for a_{hcp} and 1% for c_{hcp}). The deviation of theoretical values is slightly larger for the average atomic volumes (−1.3% for hcp-Co and +2.2% for hcp-Cu). Nevertheless, the calculations for the fcc Co-Cu system[41] yielded a similar underestimation and overestimation of the lattice parameters and atomic volumes for the pure metals (fcc-Co and fcc-Cu, respectively) as obtained here for the hcp phases. According to Ref. 41 this is primarily due to the well-known effect in that the applied PBE approximation underestimates (overestimates) the equilibrium volume of Co (Cu).

It is noted that Zhou et al.[42] have also attempted to calculate the lattice constants of the metastable hcp-Cu phase: their result was $a_{hcp\text{-}Cu} = 0.2510$ nm and $c_{hcp\text{-}Cu} = 0.6000$ nm from which $c/a = 2.39$ and $V_{hcp\text{-}Cu} = 16.37$ Å^3/atom follows. The value of $a_{hcp\text{-}Cu}$ is fairly good, but $c_{hcp\text{-}Cu}$ is evidently strongly overestimated as it can be seen also from the too large values of c/a and $V_{hcp\text{-}Cu}$ (the overestimate of the average atomic volume amounts to about 40%).

D. Composition dependence of the lattice parameters for hcp Co-Ni alloys.—The variation of the lattice constants and the average atomic volume according to Vegard's law in the hcp Co-Ni alloy system is indicated by the solid lines in Fig. A·2. It follows from the above data that when going from pure hcp-Co to pure hcp-Ni, a_{hcp} decreases by 0.7%, c_{hcp} increases by 0.4% and V_{hcp} decreases by 1%. One can see that the relative change of the lattice constants and the average atomic volume is much smaller in the Co-Ni system than in the Co-Cu system, simply due to the larger size of Cu atoms in comparison with both Co and Ni.

We have also added to Fig. A·2 the available experimental data by Taylor[43] on metallurgically prepared hcp-Co and hcp Co-Ni alloys which all contained an fcc phase as well (about 50% fcc

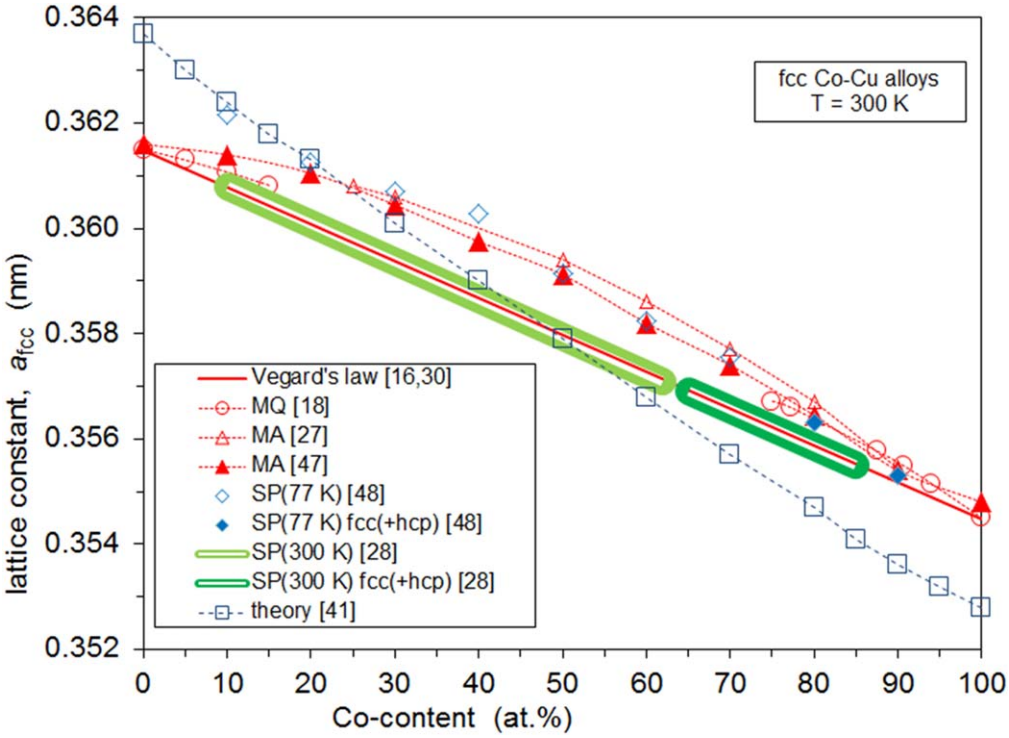

Figure A·3. Composition dependence of the lattice constant a_{fcc} for fcc Co-Cu alloys. The solid line corresponds to Vegard's law for the fcc phase in the Co-Cu system. Key to abbreviations in the legend: MQ: melt-quenching of alloys; MA: mechanical alloying of elemental powders; SP: sputtered alloy films (substrate temperature specified in brackets); fcc(+hcp): some hcp fraction is also present in the samples. The numerous experimental data from Ref. 28 are not displayed individually, just the area where they occur. The open squares represent theoretical results for fcc Co-Cu alloys.[41]

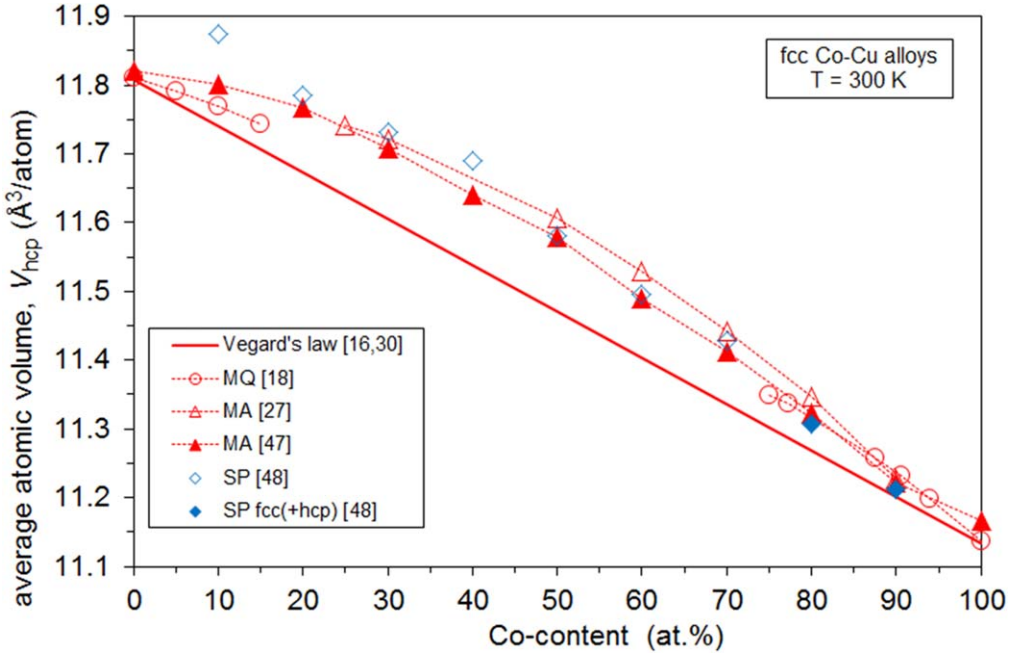

Figure A·4. Composition dependence of the average atomic volume V_{fcc} for fcc Co-Cu alloys. The solid line corresponds to Vegard's law for the fcc phase in the Co-Cu system. Key to abbreviations in the legend: MQ: melt-quenching of alloys; MA: mechanical alloying of elemental powders; SP: sputtered alloy films; fcc (+hcp): some hcp fraction is also present in the samples.

fraction was specified for the two alloy samples). The other data set added to Fig. A·2 is from the work of Rafailovic et al.[44] on electrodeposited hcp Co-Ni alloys with specified errors typically as small as ±0.0003 nm for both lattice constants. The alloy with the highest Co content (94.5 at%) was specified as fully hcp whereas a significant fcc fraction was found in the other three alloys: 82% fcc for 57 at% Co, 70% fcc for 60 at% Co and 28% fcc for 67 at% Co. All samples consisted of nanosized grains and the crystallite sizes deduced from XRD were between 10 and 20 nm for both phases.

Although the experimental data seem to show a large scatter around the Vegard's line, the agreement is actually fairly good by considering that even the largest deviations from Vegard's law

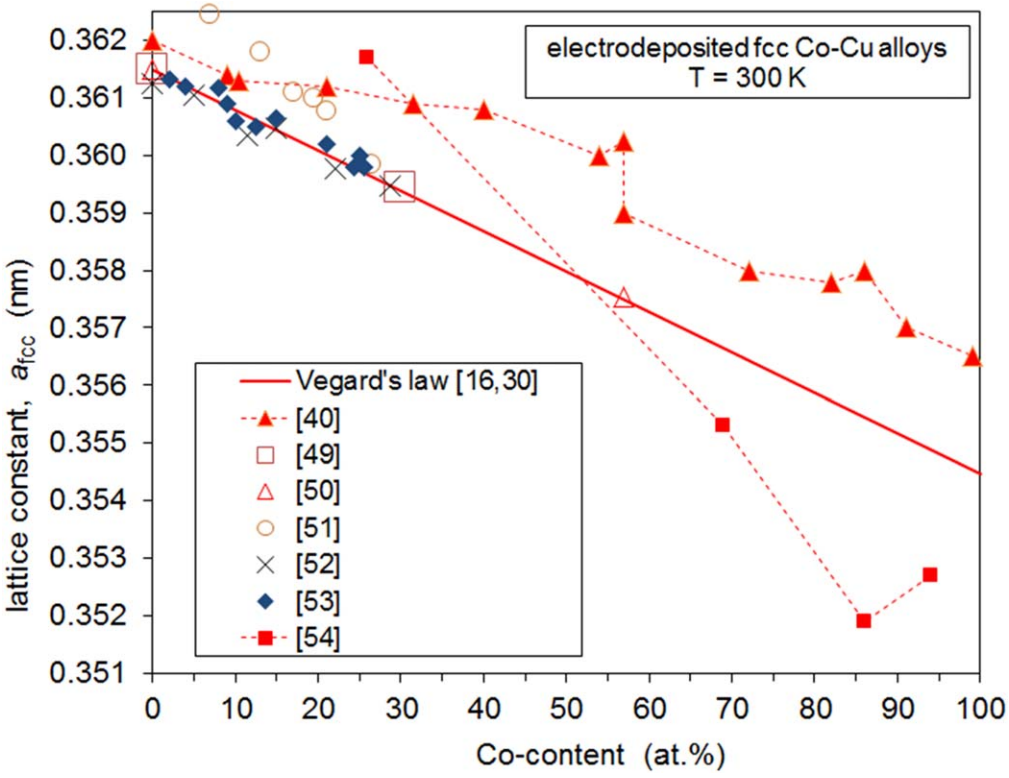

Figure A·5. Composition dependence of the lattice constant a_{fcc} for electrodeposited Co-Cu alloys. The solid line corresponds to Vegard's law for the fcc phase in the Co-Cu system. The numerous experimental data from Refs. 49 and 50 are not displayed individually, just the data for the minimum (0 at%) and maximum Co concentration; in both of these reports, about ten data points are distributed closely along the Vegard's line.

remained below about 0.5% for both the lattice constants and for the average atomic volume data.

There are two theoretical works in which the reported lattice constants are in fairly good agreement with the corresponding average experimental values listed in the last row of Table A·I: $a_{hcp\text{-}Ni} = 0.248$ nm and $c_{hcp\text{-}Ni} = 0.4092$ nm;[45] $a_{hcp\text{-}Ni} = 0.2500$ nm and $c_{hcp\text{-}Ni} = 0.408$ nm.[46] Furthermore, both sets of calculated lattice constants yield $V_{hcp\text{-}Ni}$ values which are within 1% of the standard $V_{fcc\text{-}Ni}$ value.

E. Composition dependence of the lattice parameters for fcc Co-Cu alloys.—The available experimental fcc lattice parameter data are displayed in Fig. A·3 which were obtained on Co-Cu alloys prepared by various methods (melt-quenching, mechanical alloying, sputtering). We can clearly distinguish two distinct sets of data. First, we discuss the data of Michaelsen[28] obtained on thin films prepared by sputtering on room-temperature substrates. These data points with only fcc phase fall in the light green area whereas the dark green area covers approximately the data for films containing also some hcp fraction. Apparently, all these data follow the Vegard's law. It was pointed out, however, by Michaelsen,[28] with the help of studying and modeling the XRD patterns of nanoscale Co/Cu multilayers, that these films are actually a mixture of nanoscale Co or Co-rich and Cu or Cu-rich crystallites. Namely, for such a mixture below a critical crystallite size, the XRD pattern shows a single peak between the corresponding peaks of pure fcc-Co and fcc-Cu as if it were a solid solution. On the other hand, when using sputtering for Co-Cu film preparation on a room-temperature substrate, the surface mobility of both kinds of atoms is sufficiently large to promote a segregation of the two constituents into elemental Co and Cu crystallites. The presence of superparamagnetic Co particles in these films was also demonstrated by magnetic and magnetoresistance measurements.[28] An important message of the work of Michaelsen[28] is that conventional XRD has a limit in resolving the real microstructure of nanophase alloy phases.

The next step is to look at the data of Childress and Chien[48] which were also obtained on sputtered Co-Cu alloy films, but prepared under non-equilibrium conditions. Namely, the liquid-nitrogen-cooled substrate effectively prevented the surface diffusion and, therefore, a homogeneous fcc Co-Cu solid solution could be formed which was demonstrated also by magnetic measurements. We can observe in Fig. A·3 that the lattice parameter data of these fcc Co-Cu alloys have a clear positive deviation from Vegard's law even for high Co contents where already some hcp fraction was also present. Furthermore, very similar results were obtained on mechanically alloyed Co-Cu alloys.[27,47] The observed positive deviation from Vegard's law can be ascribed to the additional volume of mixing which arises due to the heat of alloy formation of the two elements[27] which was calorimetrically measured and was in good agreement with the estimated heat of mixing. A recent theoretical calculation[41] further confirmed the magnitude of the heat of mixing. The results of a study of the lattice parameter of melt-quenched fcc Co-Cu alloys[18] are also in fairly good agreement with the positive deviation from Vegard's law obtained in Refs. 27, 47 and 48.

The theoretically calculated lattice constants for Co-Cu random solid solutions[41] are also displayed in Fig. A·3. They show a similar relation to the Vegard's law as was seen for the calculated results of hcp Co-Cu alloys for reasons mentioned in connection with Fig. A·1. As noted in Ref. 41, even the best theoretical approach applied hitherto for calculating the lattice constants of fcc Co-Cu alloys has not yet been able to reproduce the experimentally observed positive deviation from Vegard's law and this requires further theoretical efforts.

The composition dependence of the average atomic volume V_{fcc} for fcc Co-Cu alloys is displayed in Fig. A·4 and the same positive deviation from Vegard's law is revealed as for the lattice parameter in Fig. A·3.

There have been numerous reports also on the lattice parameters of electrodeposited Co-Cu alloys and these are collected in Fig. A·5. In most of these studies, a single fcc phase was only observed except

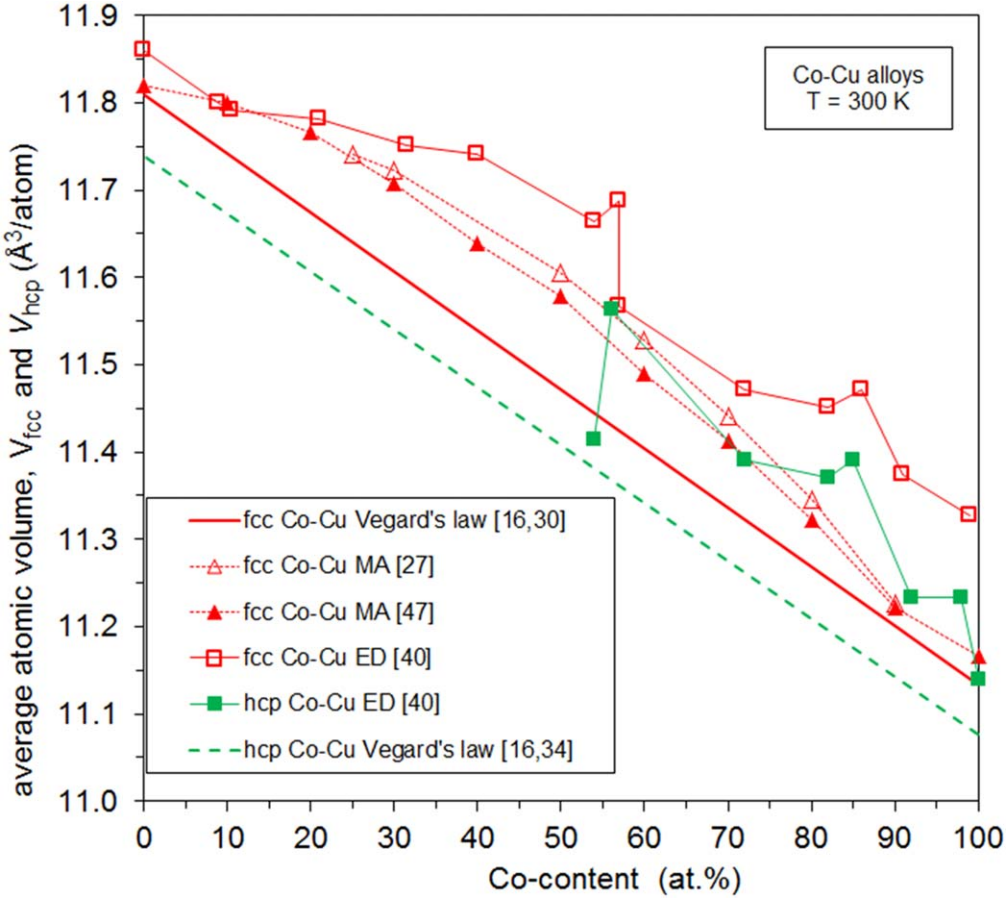

Figure A·6. Composition dependence of the average atomic volume V_{fcc} for fcc Co-Cu alloys and V_{hcp} for hcp Co-Cu alloys. The thick solid line corresponds to Vegard's law for the fcc phase in the Co-Cu system. The thick dashed line corresponds to Vegard's law for the hcp phase in the Co-Cu system. Key to abbreviations in the legend: MA: mechanical alloying of elemental powders; ED: electrodeposited alloys.

Refs. 40 and 54 in which a hcp fraction was also observed for higher Co contents. One can see that a large portion of the data[49,50,52,53] lie close to the Vegard line. In view of the discussion on the data of Michaelsen[28] displayed in Fig. A·3, it is evident that the data on electrodeposited Co-Cu alloys which follow Vegard's law indicate that these alloys were not solid solutions, but rather a mixture of nanoscale Co or Co-rich and Cu or Cu-rich crystallites. The data of Ref. 51 (open circles) and 54 (solid squares) in Fig. A·5 appear rather random with respect to the Vegard line whereas the data of Ref. 40 seem to be systematically above the Vegard line.

It was mentioned in connection with Fig. A·3 that the different preparation conditions have an influence on whether a phase mixture or a solid solution occurs in the Co-Cu system. The same should hold also for the electrodeposition process and the variety of deposition conditions applied in the studies the results of which are displayed in Fig. A·5 may be the explanation for the different behavior of the lattice parameter with respect to the Vegard's law in the different studies. To trace out, however, the influence of specific electrodeposition conditions on phase formation in these reported studies is already beyond the scope of the present work.

As noted above, the lattice parameter data of Ref. 40 seem to be systematically above the Vegard line. This behavior may resemble to some extent the true fcc Co-Cu solid solution data of Refs. 18, 27, 47 and 48 which were shown in Fig. A·3. It should be noted that the data in Ref. 40 were obtained by electron diffraction which may be generally less accurate than the XRD method used in all the other studies, but the general trend of the data of Ref. 40 still seems to be rather clear. In order to demonstrate this, Fig. A·6 shows the average atomic volume data for the fcc phase of Ref. 40 superimposed on the data obtained for the mechanically alloyed fcc Co-Cu alloys (see Fig. A·4; the other data from this figure were omitted for the sake of clarity). This comparison justifies that the electrodeposited fcc Co-Cu alloys studied in Ref. 40 may also be considered as homogeneous solid solutions.

Furthermore, we have added also the hcp phase data of Ref. 40 to Fig. A·6. These data are displayed by the green full squares and the thick dashed green line represents Vegard's law for the hcp Co-Cu system. It can be revealed in Fig. A·6 that the hcp Co-Cu data are somewhat below the fcc Co-Cu data of the same study (Ref. 40) by roughly the same amount by which the hcp Co-Cu Vegard line is shifted downwards with respect to the fcc Co-Cu Vegard line. This suggests that the hcp Co-Cu data of Ref. 40 may also be indicative of a solid solution hcp Co-Cu phase in these samples. If the alloy formation in the fcc phase requires an excess volume due to the heat of mixing of the two elements, it would not be surprising the same also for the hcp phase.

F. Composition dependence of the lattice parameters for fcc Co-Ni alloys.—The Co-Ni equilibrium phase diagram shows a complete miscibility in the fcc structure at room temperature.[1] In accordance with this, the early lattice parameter data of Taylor[43] on metallurgically processed Co-Ni alloys which are displayed in Fig. A·7 nicely follow the Vegard's line and the same holds also for the average atomic volume data (Fig. A·8).

There were several later studies[20,55–57] of the Co-Ni system both on metallurgically processed and electrodeposited alloys which also yielded lattice parameters scattered closely to the Vegard's line and, therefore, these individual data are not shown in Fig. A·7 and A·8, just their approximate range around the Vegard line is indicated in these figures by the thick green lines.

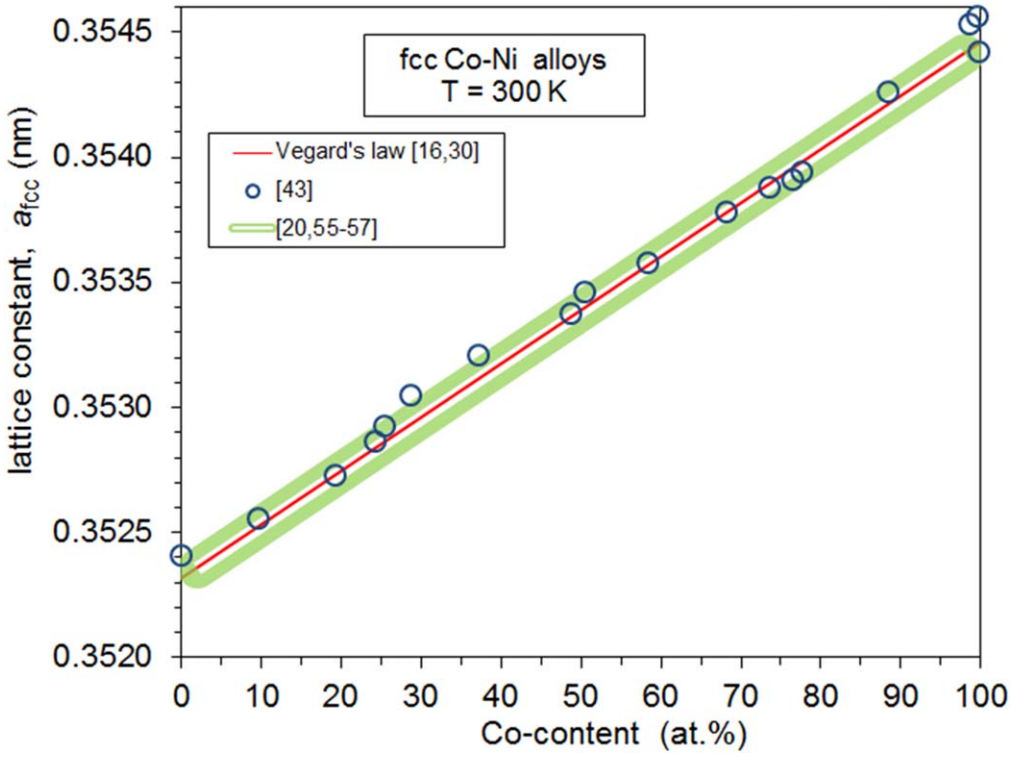

Figure A·7. Composition dependence of the lattice constant a_{fcc} for Co-Ni alloys. The solid line corresponds to Vegard's law for the fcc phase in the Co-Ni system. The open circles were obtained by Taylor[43] on metallurgically prepared alloys. The area surrounded by the thick green line indicates the area covered by the numerous data reported in Refs. 20, 55, 56 and 57 on metallurgically prepared and electrodeposited alloys.

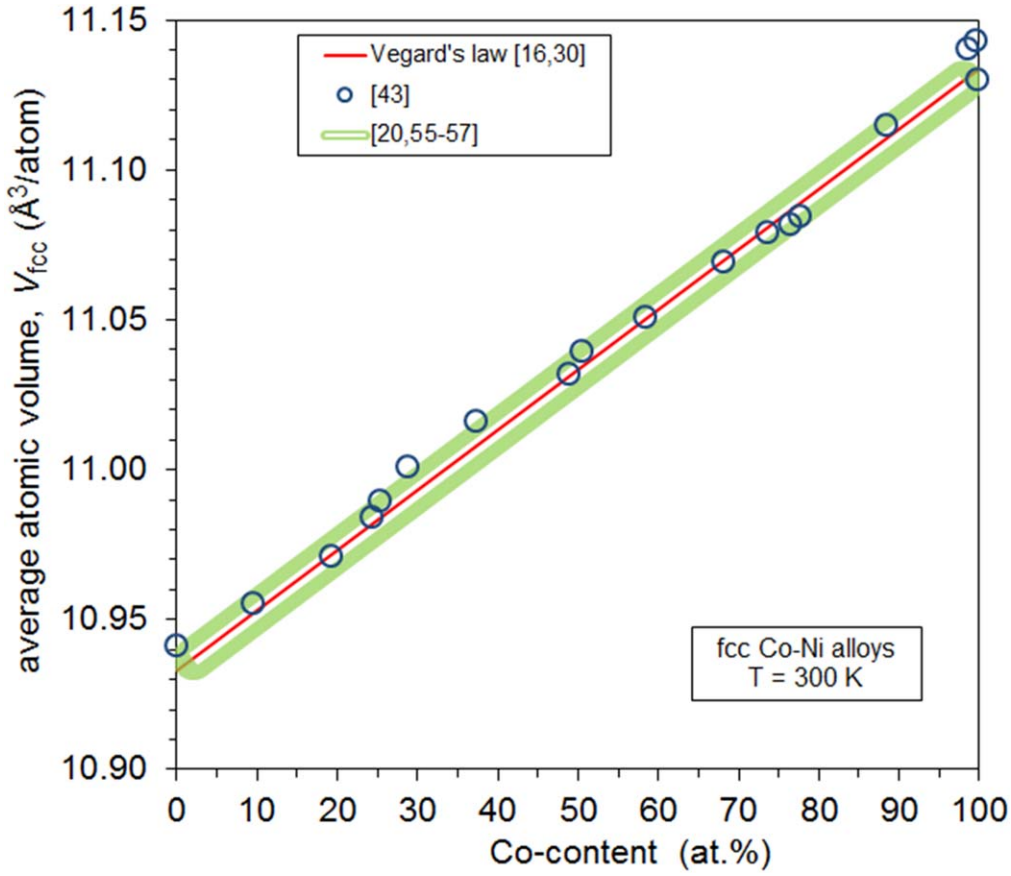

Figure A·8. Composition dependence of the average atomic volume V_{fcc} for Co-Ni alloys. The solid line corresponds to Vegard's law for the fcc phase in the Co-Ni system. The open circles were obtained by Taylor[43] on metallurgically prepared alloys. The area surrounded by the thick green line indicates the area covered by the numerous data reported in Refs. 20, 55, 56 and 57 on metallurgically prepared and electrodeposited alloys.

Some of the data of Rafailovic et al.[44] on electrodeposited Co-Ni alloys are also close to the Vegard's line, but some of them are much further; their data are, therefore, not included in these figures. These alloys consisted of a mixture of hcp and fcc crystallites with typical sizes of 10 nm. This resulted in a very low XRD intensity of most of the reflection peaks and an amorphous phase fraction was also identified in these samples. All these factors may have resulted in a larger uncertainty of the lattice parameter determination which may explain the large deviations from Vegard's law.

Anyway, there is a large amount of data confirming the Vegard's law behavior which unambiguously support that Co-Ni alloys can form a homogeneous solid solution with the fcc structure at room temperature.

ORCID

I. Bakonyi https://orcid.org/0000-0002-5873-8601

References

1. T. B. Massalski, *Binary Alloy Phase Diagrams* (Ohio, USA)(Plus Updates on CD-ROM, ASM International, Materials Park) 2nd ed. (1996).
2. I. Bakonyi, "Atomic volumes and local structure of metallic glasses." *Acta Mater.*, **53**, 2509 (2005).
3. R. Lizárraga, Fan Pan, L. Bergqvist, E. Holmström, Z. S. Gercsi, and L. Vitos, "First principles theory of the hcp-fcc phase transition in cobalt." *Sci Rep.*, **7**, 3778 (2017).
4. A. Brenner, *Electrodeposition of alloys I–II.* (Academic, New York (USA)) (1963).
5. A. W. Hull, "X-ray crystal analysis of thirteen common metals." *Phys. Rev.*, **17**, 571 (1921).
6. A. Vicenzo and P. L. Cavallotti, "Growth modes of electrodeposited cobalt." *Electrochim. Acta*, **49**, 4079 (2004).
7. M. El-Tahawy, L. Péter, J. Gubicza, L. F. Kiss, Z. S. Czigány, G. Molnár, and I. Bakonyi, "Anisotropic magnetoresistance (AMR) of cobalt: hcp-Co vs fcc-Co." *J. Magn. Magn. Mater.*, **560**, 169660 (2022).
8. V. Weihnacht, L. Péter, J. Tóth, J. Pádár, Z. Kerner, C. M. Schneider, and I. Bakonyi, "Giant Magnetoresistance in Co-Cu/Cu Multilayers Prepared by Various Electrodeposition Control Modes." *J. Electrochem. Soc.*, **150**, C507 (2003).
9. L. Péter, J. Pádár, E. Tóth-Kádár, Á. Cziráki, P. Sóki, L. Pogány, and I. Bakonyi, "Electrodeposition of Co–Ni–Cu/Cu multilayers: 1. composition, structure and magnetotransport properties." *Electrochim. Acta*, **52**, 3813 (2007).
10. B. D. Cullity and S. R. Stock, *Elements of X-ray Diffraction* 3rd ed. (Prentice Hall, Upper Saddle River, New Jersey, U.S.A.) (2001).
11. J. Gubicza, *X-ray Line Profile Analysis in Materials Science* (PA, USA)(IGI-Global, Hershey) (2014).
12. ASTM Powder Diffraction File PDF-01-077-7453 (hcp-Co); available online https://icdd.com.
13. ASTM Powder Diffraction File PDF-00-015-0806 (fcc-Co); available online https://icdd.com.
14. ASTM Powder Diffraction File PDF-00-004-0836 (fcc-Cu) available online https://icdd.com.
15. ASTM Powder Diffraction File PDF-00-004-0850 (fcc-Ni); available online https://icdd.com.
16. F. Vincent and M. Figlarz, "Quelques precisions sur les parametres cristallins et lintensite des raies Debye–Scherrer du cobalt cubique et du cobalt hexagonal." *C.R. Acad. Sci.*, **264C**, 1270 (1967).
17. E. Gómez, S. Pané, and E. Vallés, "Electrodeposition of Co–Ni and Co–Ni–Cu systems in sulphate–citrate medium." *Electrochim. Acta*, **51**, 146 (2005).
18. W. Klement Jr, "Solid solutions of gold-cobalt and copper–cobalt alloys." *Trans. Metallurg. Soc. AIME*, **227**, 965 (1963).
19. I. Bakonyi, F. D. Czeschka, L. F. Kiss, V. A. Isnaini, A. Krupp, K. Palotás, S. Zsurzsa, and L. Péter, "High-field magnetoresistance of microcrystalline and nanocrystalline Ni metal at 3 K and 300 K." *Eur. Phys. J. Plus*, **137**, 871 (2022).
20. B. G. Tóth, L. Péter, Á. Révész, J. Pádár, and I. Bakonyi, "Temperature dependence of the electrical resistivity and the anisotropic magnetoresistance (AMR) of electrodeposited Ni-Co alloys." *Eur. Phys. J. B*, **75**, 167 (2010).
21. I. Bakonyi, J. Báskay, V. A. Isnaini, L. K. Varga, L. Péter, and J. Gubicza, *(in preparation)*.
22. J. W. Retgers, "The specific gravity of isomorphous mixtures (in German)." *Z. Phys. Chem.*, **3**, 497 (1889).
23. E. Zen, "Validity of Vegard's law. *Amer.*" *Mineralogist*, **141**, 523 (1956).
24. K. T. Jacob, S. Raj, and L. Rannesh, "Vegard's law: a fundamental law or an approximation." *Int. J. Mater. Res.*, **98**, 776 (2007).
25. W. Liu, X. G. Lu, R. Ouyang, and W. S. Zheng, "Size, electronic and magnetic effects on the deviation of Retgers' law in binary FCC alloys." *J. Sol. State Chem.*, **316**, 123569 (2022).
26. S. Raju, "Volume effects of alloying: a thermodynamic perspective." *Trans. Indian Inst. Met.*, **75**, 1031 (2022).
27. C. Gente, M. Oehring, and R. Bormann, "Formation of thermodynamically unstable solid solutions in the Cu-Co system by mechanical alloying." *Phys. Rev. B*, **48**, 13244 (1993).
28. C. Michaelsen, "On the structure and homogeneity of solid solutions: The limits of conventional X-ray diffraction." *Philos. Mag. A*, **72**, 813 (1995).
29. L. Vegard, "The constitution of crystal mixtures and the space filling of atoms (in German)." *Z. Phys.*, **5**, 17 (1921).
30. P. Villars and L. D. Calvert, *Pearson's Handbook of Crystallographic Data for Intermetallic Phases* (American Society of Metals, Metals Park, Ohio) (1985).
31. H. E. Swanson, M. C. Morris, and E. H. Evans, "Standard X-ray diffraction powder patterns." *National Bureau of Standards Monograph*, **25**, 10 (1966).
32. P. Villars and L. D. Calvert, *Pearson's Handbook of Crystallographic Data for Intermetallic Phases* (American Society of Metals, Metals Park, Ohio) (1991).
33. C. Kittel, *Introduction to Solid State Physics* 6th ed. (Wiley, New York) (1986).
34. N. Takahashi, "Hétérogénéité des cristaux de cuivre produits par dépôt électrolytique sur un monocristal de laiton β poli électrolytiquement." *J. Chim. Phys.*, **50**, 624 (1953).
35. J. G. Wright and J. Goddard, "The lattice constants and magnetic anisotropy constants of electrodeposited single crystal films of hexagonal close-packed nickel." *Philos. Mag.*, **11**, 485 (1965).
36. W. Tian, H. P. Sun, X. Q. Pan, J. H. Yu, M. Yeadon, C. B. Boothroyd, Y. P. Feng, R. A. Lukaszew, and R. Clarke, "Hexagonal close-packed Ni nanostructures grown on the (001) surface of MgO." *Appl. Phys. Lett.*, **86**, 131915 (2005).
37. V. Rodríguez-González, E. Marceau, P. Beaunier, M. Che, and C. Train, "Stabilization of hexagonal close-packed metallic nickel for alumina-supported systems prepared from Ni(II) glycinate." *J. Sol. State Chem.*, **180**, 22 (2007).
38. A. S. Bolokang and M. J. Phasha, "Novel synthesis of metastable HCP nickel by water quenching." *Mater. Lett.*, **65**, 59 (2011).
39. R. T. Chiang, R. K. Chiang, and F. S. Shieu, "Emergence of interstitial-atom-free HCP nickel phase during the thermal decomposition of Ni_3C nanoparticles." *RSC Adv.*, **4**, 19488 (2014).
40. Y. Shimizu, Y. Tanabe, H. Tomita, M. Kakegawa, Y. Shimizu, Y. Tanabe, H. Tomita, and M. Kakegawa, "Crystal growth, microstructure and phase transition of electrodeposited copper-cobalt alloys as revealed by electron microscopy." *J. Met. Fin. Soc. Japan*, **29**, 131 (1978), in Japanese.
41. C. Li, H. Levämäki, R. Xie, L. Tian, Z. Dong, W. Li, S. Lu, Q. Chen, J. Ågren, and L. Vitos, "Critical assessment of Co-Cu phase diagram from first-principles calculations." *Phys. Rev. B*, **102**, 184428 (2020).
42. Y. Zhou, W. Lai, and J. Q. Wang, "Calculated electronic structure of metastable phases of Cu." *Phys. Rev. B*, **49**, 4463 (1994).
43. Taylor, "Lattice parameters of binary nickel-cobalt alloys." *J. Inst. Met.*, **77**, 585 (1950).
44. L. D. Rafailovic, W. Artner, G. E. Nauer, and D. M. Minic, "Structure, morphology and thermal stability of electrochemically obtained Ni–Co deposits." *Thermochim. Acta*, **496**, 110 (2009).
45. X. He, L. T. Kong, and B. X. Liu, "Calculation of ferromagnetic states in metastable bcc and hcp Ni by projector-augmented wave method." *J. Appl. Phys.*, **97**, 106107 (2005).
46. Z. Cheng, J. Zhu, and Z. Tang, "Magnetism of hexagonal closed-packed Ni nanowires from *ab initio* calculations." *J. Appl. Phys.*, **105**, 103906 (2009).
47. X. Fan, T. Mashimo, X. S. Huang, T. Kagayama, A. Chiba, K. Koyama, and M. Motokawa, "Magnetic properties of Co-Cu metastable solid solution alloys." *Phys. Rev. B*, **69**, 094432 (2004).
48. J. R. Childress and C. L. Chien, "Reentrant magnetic behavior in fcc Co-Cu alloys." *Phys. Rev. B*, **43**, 8089 (1991).
49. Y. Ueda and M. Ito, "Magnetoresistance in Co–Cu Alloy films formed by electrodeposition method." *Jpn. J. Appl. Phys.*, **33**, L1403 (1994).
50. H. Zaman, A. Yamada, H. Fukuda, and Y. Ueda, "Magnetoresistance effect in Co-Ag and Co-Cu alloy films prepared by electrodeposition." *J. Electrochem. Soc.*, **145**, 565 (1998).
51. Ö. F. Bakkaloglu, I. H. Karahan, H. Efeoglu, M. Yildirim, U. Cevik, and Y. K. Yogurtcu, "Magnetic studies on electrodeposited $Cu_{1-x}Co_x$ alloy films." *J. Magn. Magn. Mater.*, **190**, 193 (1998).
52. E. Gómez, A. Llorente, and E. Vallés, "Obtention and characterisation of cobalt +copper electrodeposits from a citrate bath." *J. Electroanal. Chem.*, **495**, 19 (2000).
53. R. López Antón, M. L. Fdez-Gubieda, A. García-Arribas, J. Herreros, and M. Insausti, "Preparation and characterisation of Cu–Co heterogeneous alloys by potentiostatic electrodeposition." *Mater. Sci. Eng. A*, **335**, 94 (2002).
54. M. R. Khelladi, L. Mentar, A. Azizi, L. Makhloufi, G. Schmerber, and A. Dinia, "The potential dependence of Co–Cu alloy thin films electrodeposited on n-Si(100) substrate." *J. Mater. Sci., Mater. Electron.*, **23**, 2245 (2012).
55. W. B. Pearson and L. T. Thompson, "The lattice spacings of nickel in solid solutions." *Can. J. Phys.*, **35**, 349 (1957).
56. M. Hlinička and I. Karmazin, "New lattice parameter study of Ni-Co alloys with respect to ordering in Ni_3Co." *Scripta Metall.*, **8**, 1029 (1974).
57. J. Bandyopadhyay and K. P. Gupta, "Low temperature lattice parameter of nickel and some nickel-cobalt alloys and Grüneisen parameter of nickel." *Cryogenics*, **17**, 345 (1977).